

# Optimal seismic retrofit method for reinforced concrete columns with wing walls

Yousok Kim<sup>a</sup>, Su A. Lim<sup>b</sup>, Hyo Seon Park<sup>b,\*</sup>

<sup>a</sup> Department of Architectural Engineering, Hongik University, Sejong, South Korea

<sup>b</sup> Department of Architectural Engineering, Yonsei University, Seoul, South Korea

## ARTICLE INFO

### Keywords:

Wing walls  
Reinforced concrete columns  
Seismic retrofit  
Reinforce concrete frame

## ABSTRACT

Seismic retrofit of reinforced concrete (RC) columns using wing walls can be used to improve the shear and flexural strength of the column through a relatively simple process. However, the feasibility and efficiency of the seismic retrofitting of RC frames with wing walls heavily depends on the selection of number of columns to be retrofitted, the cross-sectional dimensions of wing walls, and the quantity of re-bars of the wing wall. In this study, an optimal seismic retrofit design method is proposed to minimize not only the initial retrofit cost but also the earthquake-induced damage expected during the life cycle of the building. The seismic performance of structures before and after the application of the retrofit has been verified with the comparison of four response parameters: pushover curves, the inter-storey drift ratios, the energy dissipation capacities, and failure modes. The proposed retrofit method is applied to seismic retrofit of a six-storey RC building example and an actual RC building structure in use. For the retrofit of actual building structure, with an initial retrofit weight of 70.85 kN, which corresponds to 1.85% of the weight of the non-retrofitted building, the energy dissipation capacity was increased by 3.02 times and the life cycle cost (LCC) of the retrofit was reduced to 69.47% of the required LCC for the non-retrofitted building. In addition, it has been confirmed that no storey collapse occurred in collapse prevention level, which indicates the most severe failure mechanism of a structure due to an earthquake.

## 1. Introduction

During and prior to the 1980 s, when the concept of seismic design had not yet been established in developing countries, buildings were designed without consideration of seismic performance. Accordingly, those buildings tended to suddenly collapse under an external force, such from an earthquake, due to displacement capacity not being considered [1]. In particular, the sudden failure of columns, which are structural members bearing vertical loads, leads to failure to support building weight. This causes the collapse of the entire building and enormous human and structural damages [2–4]. To prevent such damage, various seismic retrofit studies have been conducted on old buildings that have not been seismically retrofitted, and the number of seismically retrofitted buildings is therefore on the rise [5–10].

Seismic retrofit methods, which are practically applicable to the improvement of the seismic performance of existing buildings, can be classified as either strength and stiffness retrofit methods or ductility retrofit methods. Seismic retrofitting of building structures with steel bracings and bearing walls is a representative strength and stiffness retrofit method. Although this method can sufficiently improve seismic

performance, a building may still have brittle behavior, which can result in sudden failure [11–13]. On the other hand, ductility retrofit using carbon fiber jackets or steel jackets has a confinement effect on structural members, which partially improves strength and significantly enhances ductility capacity. However, the number of structural members to be retrofitted must be increased, which increases both the working duration and retrofit cost [14–17]. For this reason, many studies have attempted to find the most appropriate retrofit method that can increase strength and ductility capacity satisfactorily.

Among the many column retrofit methods, seismic retrofit of reinforced concrete (RC) columns with wing walls involves installation of RC walls, which are not so large as to be regarded as shear walls, at both sides of a column. As this method can efficiently improve the shear and flexural strength of the column through a relatively simple process, its effectiveness has been verified through many studies and experiments. The behaviors of columns reinforced by wing walls began to be formulated as early as the 1970 s, and various experimental studies have been performed up to now.

Among the studies in the 1970 s, Higashi et al. carried out an experimental study to identify the shear strength of a wing wall [18–21].

\* Corresponding author.

E-mail address: [hspark@yonsei.ac.kr](mailto:hspark@yonsei.ac.kr) (H.S. Park).

<https://doi.org/10.1016/j.engstruct.2020.110390>

Received 22 April 2019; Received in revised form 5 November 2019; Accepted 12 February 2020

Available online 28 February 2020

0141-0296/ © 2020 Elsevier Ltd. All rights reserved.

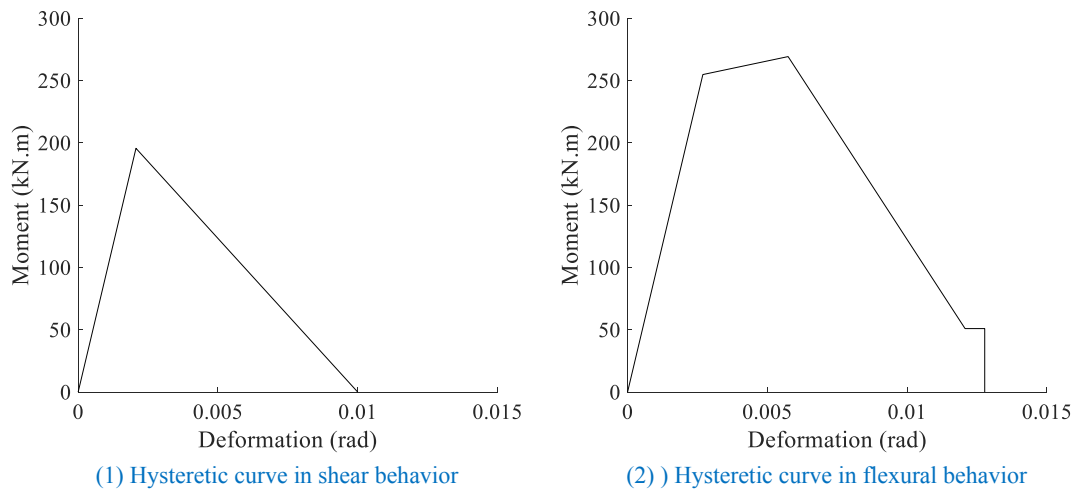


Fig. 1. Hysteretic curve of the first floor internal column of the example building.

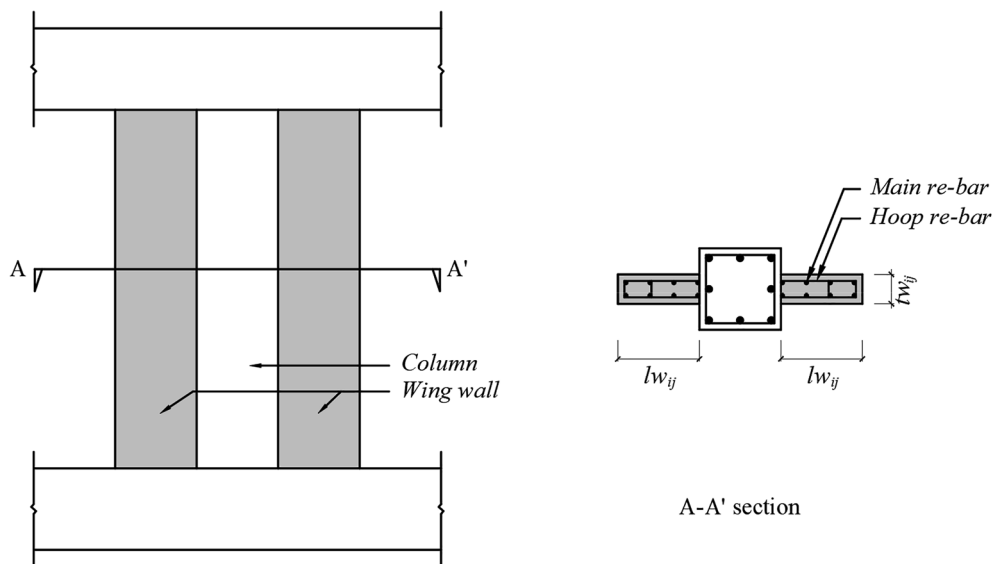


Fig. 2. Column retrofitted by wing walls.

Table 1  
Performance level and damage state in terms of permissible drift ratios.

Performance level	Damage state	Permissible drift ratios (%)
I	None	$\Delta < 0.2$
II	Slight	$0.2 < \Delta < 0.5$
III	Light	$0.5 < \Delta < 0.7$
IV	Moderate	$0.7 < \Delta < 1.5$
V	Heavy	$1.5 < \Delta < 2.5$
VI	Major	$2.5 < \Delta < 5.0$
VII	Destroyed	$0.5 < \Delta$

In 2001, a strength equation for a wing wall reinforced column was proposed in the seismic evaluation standard of JBDPA (Japan Building Disaster Prevention Association) [22]. A series of experiments was conducted on wing walls from 2007 to 2010. These experiments mainly measured the shear strength of wing walls with diverse thicknesses and lengths [23–26]. In 2009, a method of installing a wing wall at only one side of a column was experimentally examined. Cyclic loads were

applied to 4 wing wall specimens with different shapes. The experimental results demonstrated the behaviors of the reinforced specimen according to loading directions [27]. Although the failure modes of loading directions were different, the wing wall prevented the main re-bar of the wing wall from yielding in every specimen. In 2010, another experiment was conducted to identify stress after flexural yielding. Six column specimens reinforced by wing walls at both sides were used; they were differentiated according to the thickness and length of wing walls and the confinement of wing wall ends [28]. In the experiment, when the wing walls were 1/4 as thick as the column, the compressive fracture of concrete and the buckling of re-bar occurred at wing wall ends. Besides, the strength drastically decreased after reaching its peak. When the wing walls were 3/8 as thick as the column, the strength did not show such a drastic decrease. Although the strength decreased at different rates according to thickness, every specimen had sufficient ductility capacity and showed flexural failure behavior, indicating a seismic retrofitting effect of the wing walls. Liu et al. performed an experiment in which the thickness and length of a wing wall were set as variables and a lateral force was applied. When the length of one side of a wing wall was twice that of the column depth, the resistant force for lateral force doubled and the shearing strength increased by a factor of

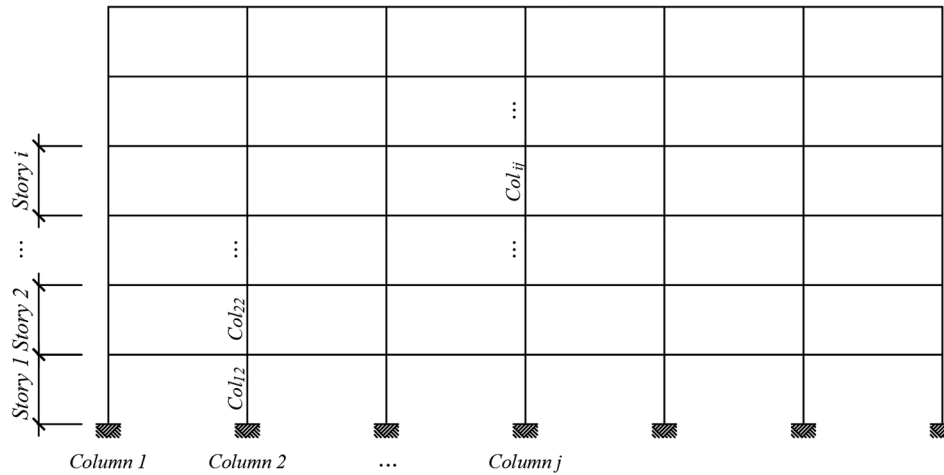
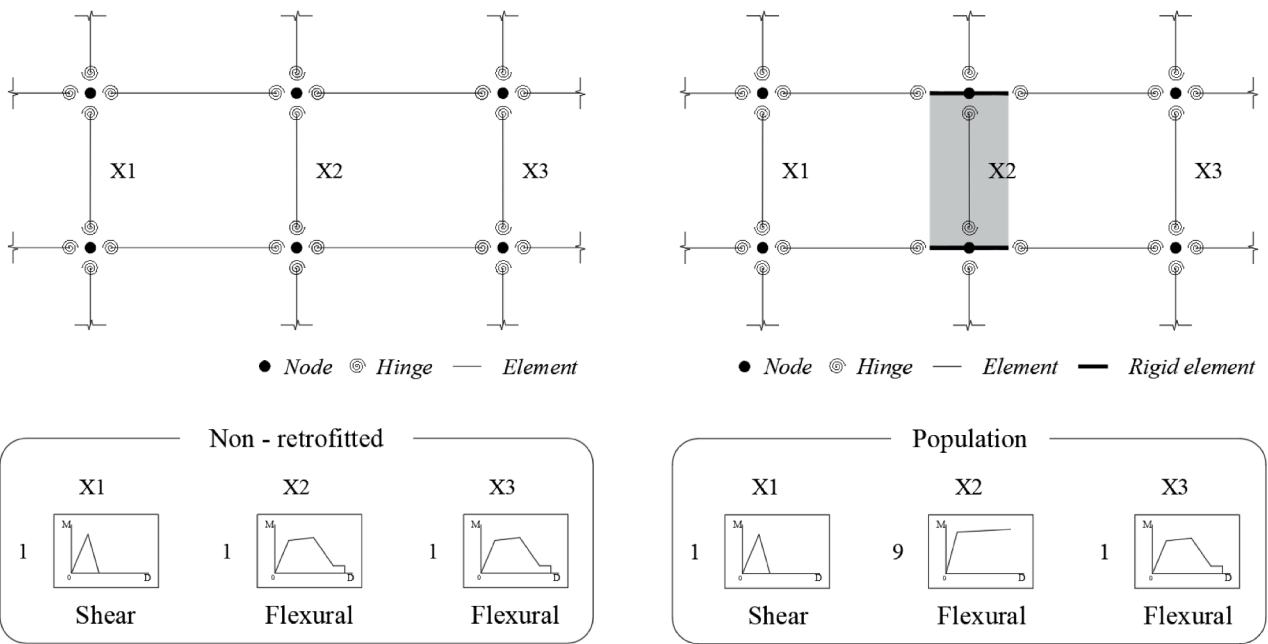


Fig. 3. Columns to be retrofitted with wing walls.



(1) Structure before retrofitting

(2) A population structure

Fig. 4. Numerical analysis model in the case of before retrofitting and random population.

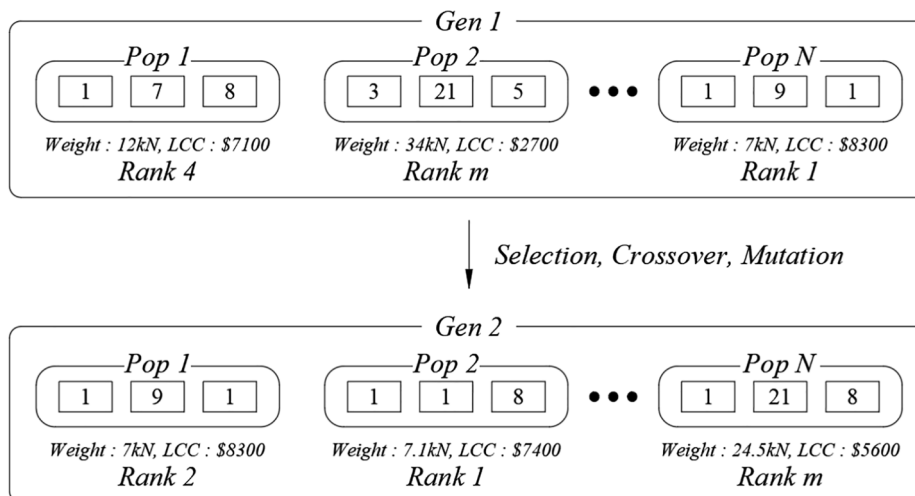


Fig. 5. The evolution process of NSGA-II.

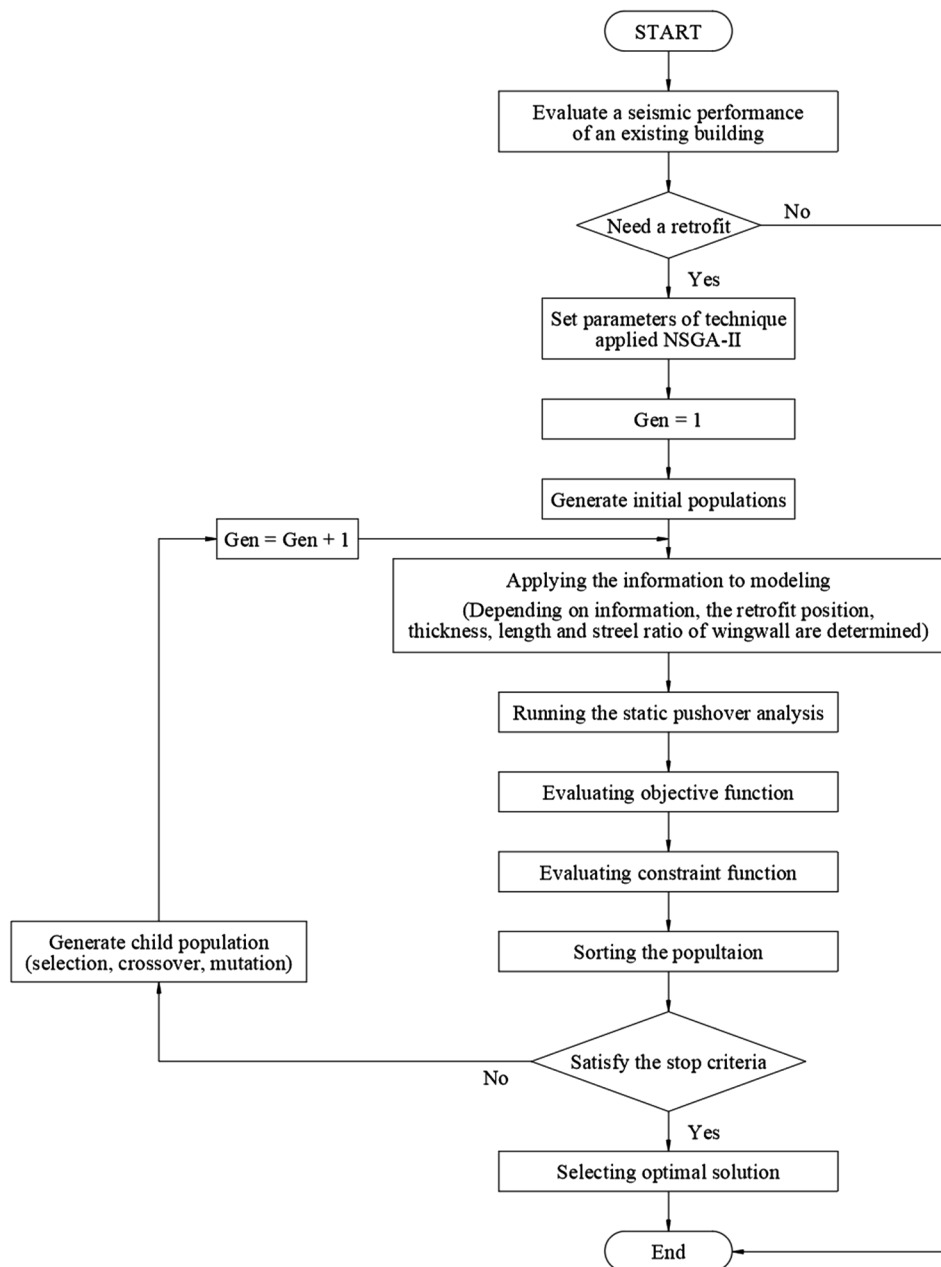


Fig. 6. The procedure of the proposed optimal seismic retrofit method.

approximately 4 to 5 [29]. Chang et al. experimentally examined the behaviors of a column reinforced by wing walls installed at both sides by focusing on whether the transverse re-bar of a wing wall was placed through the column [30].

There have been many experimental studies that deal with the retrofit effect of wing walls on a column. However, when a seismic retrofit method using wing walls is applied to an actual building, number of columns to be retrofitted (retrofit points), the cross-sectional dimensions of wing walls (wing wall section), and the quantity of re-bars of the wing wall are determined by an engineer's experience and intuition. This factor degrades the efficiency of the retrofit with wing walls. Accordingly, this study proposes a retrofit design method to determine optimal number of retrofit points, wing wall sections, and re-bar quantity to satisfy a user's purpose, as in the case of seismic performance of a target building.

In this study, to improve the feasibility and efficiency of the seismic retrofitting of RC frames with wing walls, an optimal seismic retrofit

design method is proposed. In the proposed retrofit design method, in order to minimize not only the initial retrofit cost but also the earthquake-induced damage expected during the life cycle of the building [31,32], both the initial cost and the life-cycle cost (LCC) for the seismic retrofit of RC frames with wing walls have been formulated into objective functions and minimized by a multi-objective optimization algorithm [7,33–36]. The seismic performances and constructability of the retrofitted building have been checked by four constraint conditions: a constraint on the storey drift ratio of a structure satisfying a target performance, a constraint on failure mode to prevent the shear failure of the retrofitted structure, a constraint on the yield strength of the floor, and a constraint on cross-sectional dimensions of wing walls to ensure constructability. Nonlinear analyses of the building before and after retrofitting were performed using OpenSees[37]. For the purpose of verification, the proposed method was applied to seismic retrofit of a six-storey RC structure used by Ozel and Guneyisi [13]. Finally, the performance of the proposed retrofit design method was

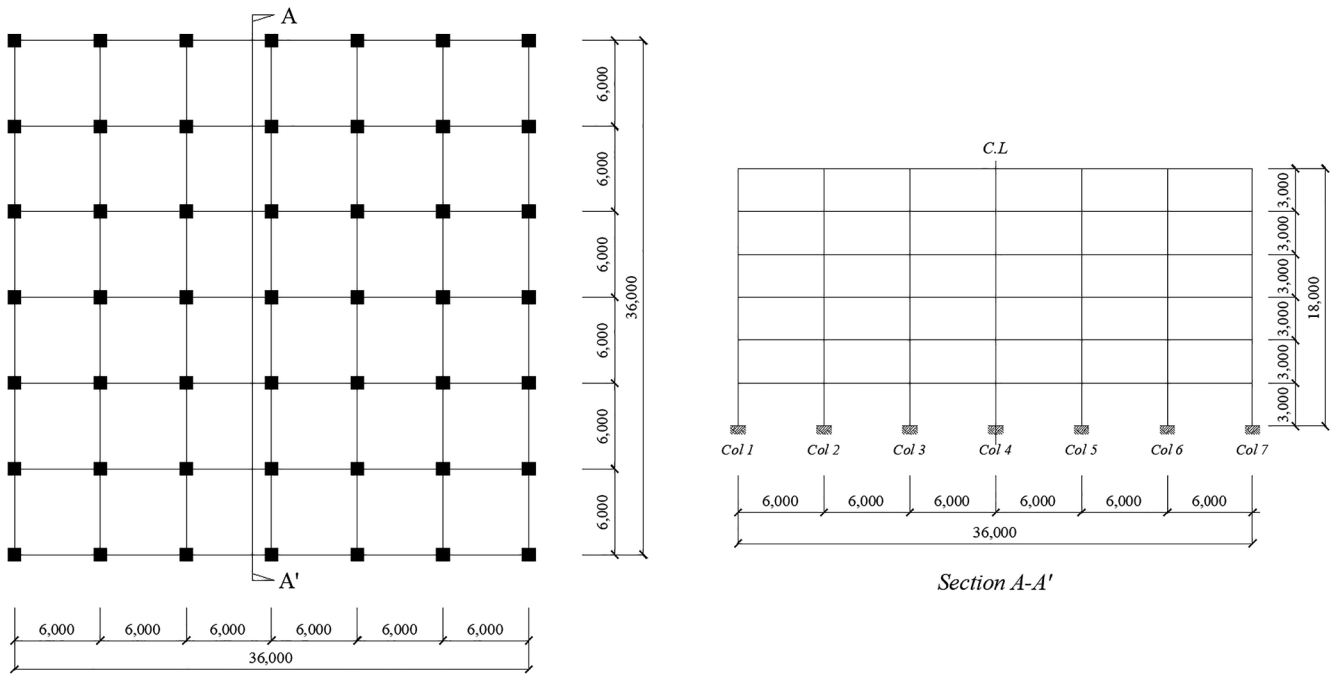


Fig. 7. Plan and elevation of the six-storey RC structure.

illustrated by seismic retrofit design of an actual six-storey six-span RC frame structure.

**2. Numerical analysis models for the existing members and a column retrofitted by wing walls**

*2.1. Numerical analysis model of the existing member*

To implement and verify the optimal seismic retrofit method using wing walls, a lumped plasticity model, which simulates the nonlinear behaviors of a member by inputting the hysteretic curves of the member into the hinges at both ends [38–40], is used in this study. The flexural and shear strengths of columns and beams before retrofitting were evaluated using equations from the BCJ (Building Center of Japan) [41].

The detailed formulas can be found in Appendix A. Hinge parameters for hysteretic curve setting of members, including flexural and shear strength, were calculated according to FEMA356. According to FEMA356, the characteristics of hysteretic curves of members can be classified according to the failure modes of members. Since the nonlinear behavior of a member changes after the yield point depending on the failure mode, it is important to identify and reflect the failure mode

of the member. The failure mode of a member can be identified based on the ratio of shear strength  $Q_{su}$  to flexural strength  $Q_{mu}$ , as expressed in Eq. (1). In this study, when calculating the flexural and shear strengths of the column, the effects of the variable axial force were not considered and only the effect of self-load are taken into account.

$$Q_{su}/Q_{mu} \tag{1}$$

When the ratio obtained by Eq. (1) exceeds 1.0, the member is a flexural, showing hysteretic characteristics of strain hardening and strength decrease after maximum strength. When the ratio is less than 1.0, the member is shear, showing a drastic decrease of strength after shear strength. Fig. 1(1) and (2) show the skeleton curves of shear failure and flexural failure columns, respectively. In the case of the shear failure type member, a sudden decrease in strength occurs immediately after the maximum strength is reached, whereas in the case of a flexural failure member, a slight increase in strength due to the hardening of the strain after reaching the maximum strength, and shows the failure after the strength decrease. In the case of flexural failure members, the point of strength drop is different depending on the characteristics of the members, and the evaluation for this used the method proposed in FEMA356.

**Table 2**  
Details of the column section of the six-storey RC structure.

Column	Col <sub>11</sub> , Col <sub>21</sub> , Col <sub>32</sub> ~ Col <sub>34</sub> , Col <sub>42</sub> ~Col <sub>44</sub>	Col <sub>12</sub> ~Col <sub>14</sub> Col <sub>22</sub> ~Col <sub>24</sub>	Col <sub>31</sub> , Col <sub>41</sub> , Col <sub>52</sub> ~ Col <sub>54</sub> , Col <sub>62</sub> ~Col <sub>64</sub>	Col <sub>42</sub> ~Col <sub>44</sub>
Section				
Re-bar	8 - D16	8 - D18	8 - D14	8 - D14
Stirrup	D8 @200	D8 @200	D8 @200	D8 @200

**Table 3**  
The ratio in Eq. (1) of columns in the six-storey RC office building example.

	Col 1	Col 2	Col 3	Col 4	Col 5	Col 6	Col 7
Storey 1	0.98	0.77	0.77	0.77	0.77	0.77	0.98
Storey 2	1.05	0.81	0.81	0.81	0.81	0.81	1.05
Storey 3	1.22	0.92	0.92	0.92	0.92	0.92	1.22
Storey 4	1.38	1.02	1.02	1.02	1.02	1.02	1.38
Storey 5	1.56	1.27	1.27	1.27	1.27	1.27	1.56
Storey 6	1.97	1.71	1.71	1.71	1.71	1.71	1.97

**Table 4**  
The ratio in Eq. (1) of beams in the non-retrofitted of six-storey RC office building example.

	Bay 1	Bay 2	Bay 3	Bay 4	Bay 5	Bay 6
Floor 2	1.32	1.30	1.30	1.30	1.30	1.32
Floor 3	1.30	1.27	1.27	1.27	1.27	1.30
Floor 4	1.44	1.39	1.38	1.38	1.39	1.44
Floor 5	1.69	1.57	1.56	1.56	1.57	1.69
Floor 6	1.91	1.90	1.90	1.90	1.90	1.91
Floor 7	3.54	2.78	2.75	2.75	2.78	3.54

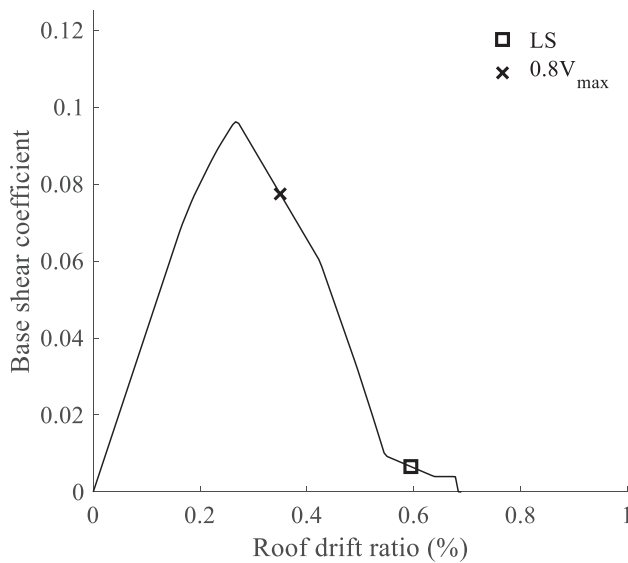


**Fig. 8.** Pushover curves for the six-storey RC office building example.

2.2. Numerical analysis model of column retrofitted by wing walls

As shown in Fig. 2, the retrofit method for a column using wing walls adds RC walls with the same shape at both sides of the column. The flexural and shear strengths of the column are effectively improved by the wing walls. In particular, if a column retrofitted by wing walls has a bending failure, its hysteretic characteristic includes an increase of the strength, even after the flexural yield strength. However, as shown by Kabeyasawa’s experiment, if the reinforcements in the wing wall are not properly confined, the resisting force drastically decreases after its peak due to the concrete crushing at the end of the wing wall [28]. Accordingly, in order to ensure sufficient development of the seismic retrofit of wing walls, it is assumed that the reinforcements at the ends of wing walls were confined, and the stiffness of the ascending part after the flexural yield strength (the hardening branch) was 0.1% of the initial stiffness. In this study, Eqs. (2) and (3), which were

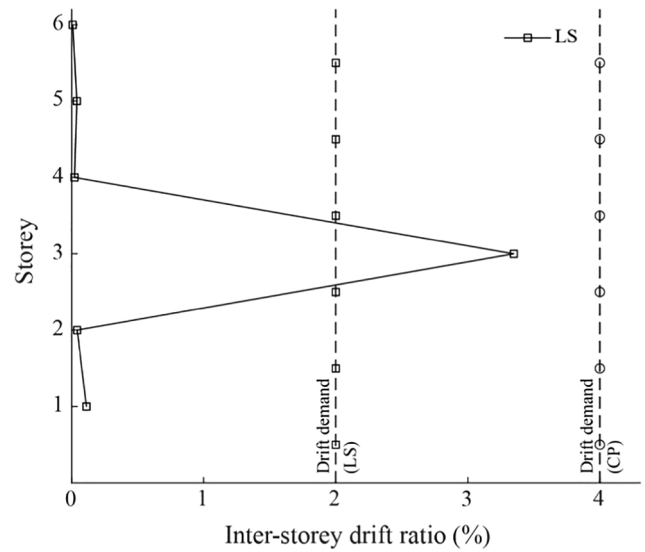


**Fig. 9.** Storey drift ratios of the six-storey RC office building example.

proposed by JBDPA [22], were used to calculate the flexural and shear strengths of the column retrofitted by wing walls.

The flexural yield strength of the column retrofitted with wing walls is estimated based on the flexural bending theory of the cross section. (Eq. (2), Appendix B).

$$M_y = \sum (a_t \times \sigma_y \times j_t) + N \times j_N \tag{2}$$

where  $a_t$  is the cross-sectional area of a tension re-bar,  $\sigma_y$  is the yield strength of the re-bar,  $j_t$  is the distance between the center of the tension re-bar and the center of compression area of concrete,  $N$  is the axial force acting on the column retrofitted by wing walls, and  $j_N$  is the distance between the application point of the axial force and the center of the compression area on the concrete.

The ultimate shear strength of the column retrofitted by wing walls is separately calculated for the wing wall and column parts, as described in Eq. (3).

$$Q_{su} = Q_{suw} + Q_{suc} + 0.1N \tag{3}$$

where  $Q_{suw}$  and  $Q_{suc}$  are the shear strength of the wall element and the shear strength of the column element [22], respectively. The explicit expressions for  $Q_{suw}$  and  $Q_{suc}$  can be found in JBDPA [22] are listed in the Appendix. The ratio of Eq. (1) can be obtained from the flexural strength and shear strength of a wing wall, which are calculated by Eqs. (2) and (3). The ratio indicates the failure mode when the wing wall shows nonlinear behavior.

The failure mode of all columns retrofitted by the wing-wall is designed as flexural failure, and after the maximum strength, the strength is not deteriorated and is modeled as a bilinear skeleton curve corresponding to stiffness of 0.1% of the initial stiffness. Therefore, the shear failure type column retrofitted by the wing-wall improves the deformation capacity along with the improvement of stiffness and strength.

3. Optimal seismic retrofit method using wing walls

In this paper, the retrofit design method for columns using wing walls has been formulated into a multi-objective optimization problem. The retrofit design method minimizes two objective functions of the initial retrofit cost and the LCC for the retrofitted RC frames with wing

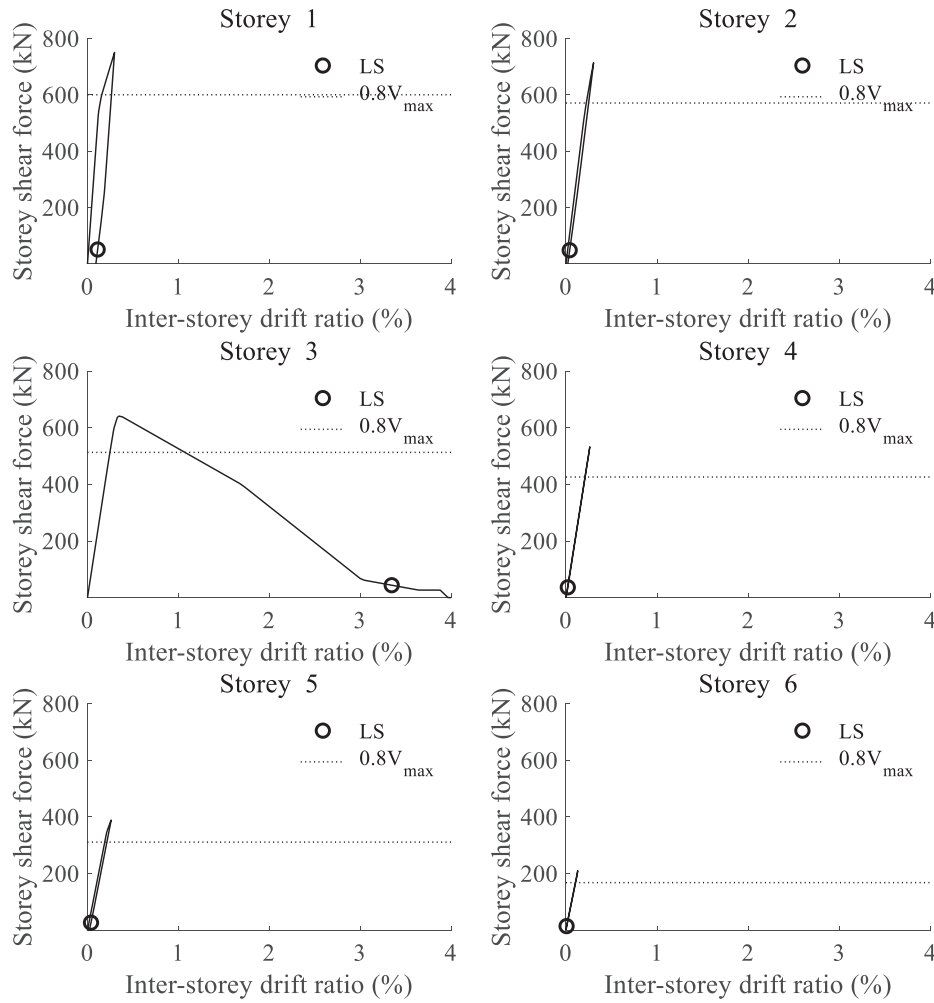


Fig. 10. Storey failure of the six-storey RC office building example in LS level.

walls while satisfying four constraints on the storey drift ratio, failure mode, the yield strength of the floor, and cross-sectional dimensions of wing walls.

### 3.1. Objective functions

If a low initial retrofit cost is planned, the building is very likely to be damaged by an earthquake, which will occur during the life cycle after retrofitting. On the other hand, if a high initial retrofit cost is planned, the building is less likely to be damaged by an earthquake during the life cycle. In other words, the initial retrofit cost is conceptually opposite to the LCC. Accordingly, a designer or user must determine a reasonable retrofit solution by considering a balance between initial cost and LCC. The two objective functions for total weight of wing walls for the retrofit, which corresponds to the initial retrofit cost, and the LCC consisting of a retrofit solution are given in Eqs. (4) and (5), respectively.

$$\text{Minimize } f_1 = \sum_{i=1}^n \sum_{j=1}^m w_{ij} \quad (4)$$

$$\text{Minimize } f_2 = \frac{v}{\lambda} (1 - e^{-\lambda t}) \sum_{i=1}^k C_i P_i \quad (5)$$

$f_2$  is the cost of losses incurred by the expected earthquake during the life cycle of the building, and a method presented by Wen and Kang [31], Liu [32,42] et al. has been used.  $v$ ,  $\lambda$ ,  $t$ ,  $k$ , and  $C_i$  are annual occurrence rate of major seismic events modeled by a Poisson process, annual monetary discount rate, service life of a retrofitted structure, number of seismic damage states considered, the cost function of  $i$ th seismic damage state, respectively.  $P_i$  is probability of  $i$ th seismic damage state, and as defined in Eqs. (6)–(8), it is calculated based on the inter-storey drift ratio  $\Delta$  obtained through nonlinear static analysis.

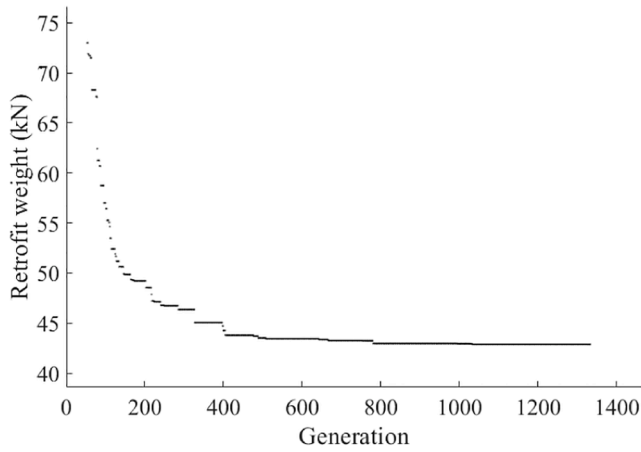
$$P_i = P(\Delta > \Delta_{i,\min}) - P(\Delta > \Delta_{i,\max}) \quad (6)$$

Here,  $\Delta_{i,\min}$  and  $\Delta_{i,\max}$  are the upper limit and lower limit of permissible drift ratio, which correspond to  $i$ -th damage state defined in FEMA227, and this can be seen in the Table. 1  $P(\Delta > \Delta_{i,\min})$  and  $P(\Delta > \Delta_{i,\max})$  represent annual exceedance probability of exceeding  $\Delta_{i,\min}$  and  $\Delta_{i,\max}$  within  $t$  years respectively, and can be obtained by Eqs. (7) and (8).

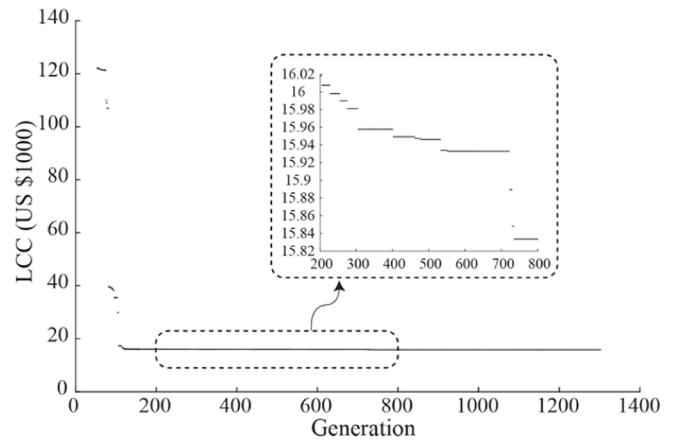
$$P(\Delta > \Delta_{i,\min}) = -\frac{1}{v \times t} \{\ln[1 - P_i(\Delta > \Delta_{i,\min})]\} \quad (7)$$

$$P(\Delta > \Delta_{i,\max}) = -\frac{1}{v \times t} \{\ln[1 - P_i(\Delta > \Delta_{i,\max})]\} \quad (8)$$

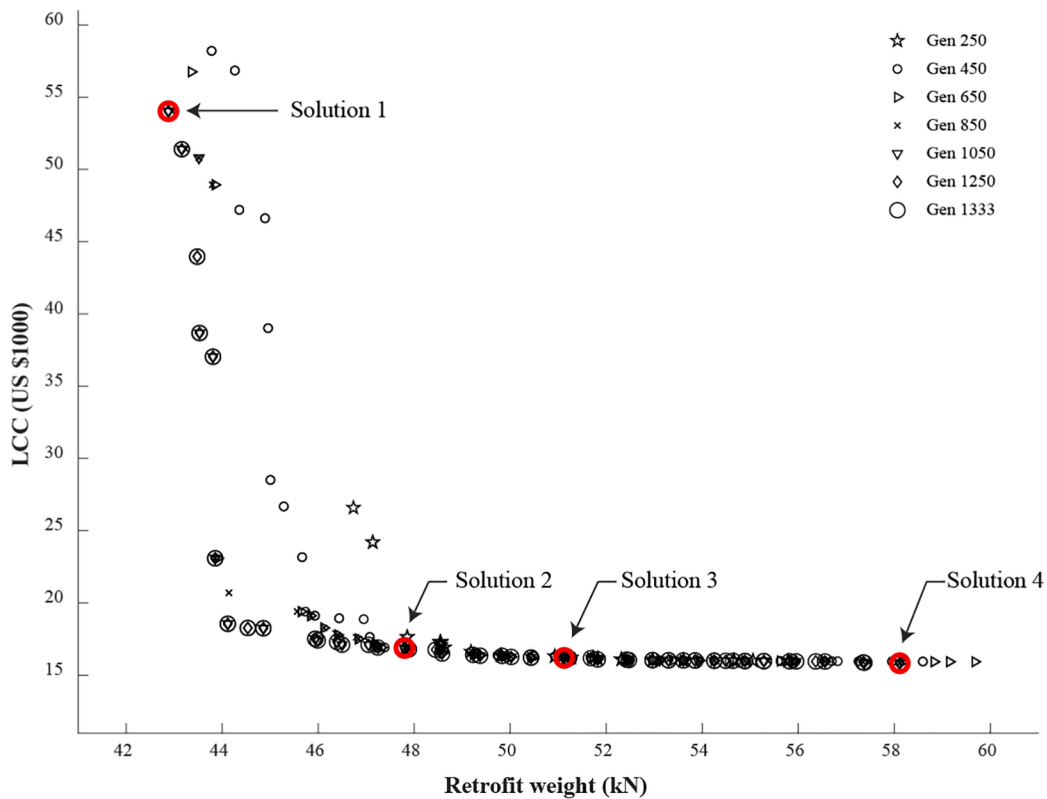
In this study, to calculate  $P_i(\Delta > \Delta_i)$ , two seismic levels with 50 year



(1) Convergence curve for retrofit weight



(2) Convergence curve for LCC



(3) Pareto solutions by generation

Fig. 11. The evolution process of NSGA-II.

exceedance probabilities of 10%, and 2% are used, respectively. Through pushover analysis, pairs of maximum inter-storey drift ratios and their exceedance probabilities at all seismic levels can be obtained, and through regression analysis, we obtain a function representing  $P_i(\Delta > \Delta_i)$ , annual exceedance probability. When performing regression analysis,  $P_i(\Delta > \Delta_i)$  is assumed to follow generalized extreme value distribution (GEVD). For relevant factors and further details of the method can be found in [31].

### 3.2. Design variables

As illustrated in Fig. 2, a wing wall with a length of  $lw_{ij}$  and thickness of  $tw_{ij}$  consists of main re-bar and hoop re-bar. In this study, retrofit points, wing wall section, and the quantity of re-bars have been used as design variables in the multi-objective optimization since the design strength depends on the length, thickness, and amount of re-bars of a wing wall. As defined in Introduction, the retrofit points and wing wall

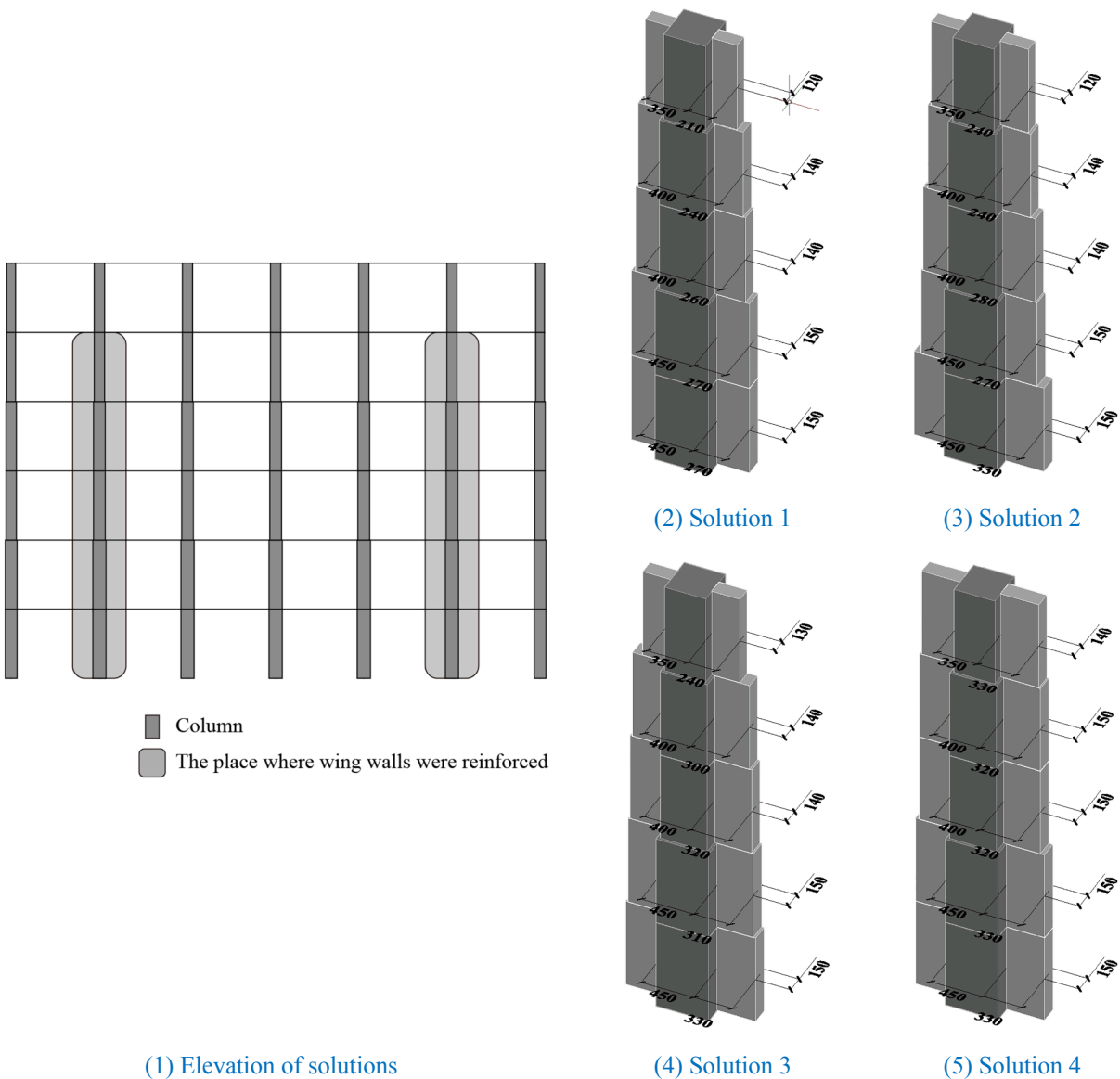


Fig. 12. The shape of Pareto solutions of 6-storey RC example.

Table 5

The ratio in Eq. (1) of beams in the solution 4 of six-storey RC office building example.

	Bay 1	Bay 2	Bay 3	Bay 4	Bay 5	Bay 6
Floor 2	1.24	1.22	1.30	1.30	1.22	1.24
Floor 3	1.22	1.20	1.27	1.27	1.20	1.22
Floor 4	1.36	1.31	1.38	1.38	1.31	1.36
Floor 5	1.60	1.48	1.56	1.56	1.48	1.60
Floor 6	1.80	1.79	1.90	1.90	1.79	1.80
Floor 7	3.54	2.78	2.75	2.75	2.78	3.54

section represent number of columns to be retrofitted and cross-sectional dimensions of wing walls, respectively. For the retrofit point, since wing walls are installed at both sides of a column, it is difficult to apply a wing wall to peripheral columns. For this reason, such peripheral columns were excluded from retrofitting. As shown in Fig. 3, in this study, the  $j$ -th column of the  $i$ -th floor was referred to as  $Col_{ij}$ , for convenience sake.

In this study, the thickness of the wing wall,  $tw_{ij}$ , was set to vary from 1/3 to 1/2 that of the column by increments of 10 mm. The minimum length, which enabled the wing wall to play a structural role, was 450 mm (that is, the sum of the lengths of two wing walls installed at each side of a column). Accordingly, the length,  $lw_{ij}$ , was set to vary from 450 mm by increments of 20 mm up to 1.5 times the maximum length of the column. Finally, as for the amount of re-bars, JBDPA [21] specified the minimum amount of both longitudinal and transverse re-bar as 0.25% of the wing wall section. Accordingly, the amount of re-bar was set to vary from 0.25% to 1% by increments of 0.25%, which resulted in 4 types. In addition, among the physical properties of the wing wall, the compressive strength of concrete has been fixed 30 MPa. For reinforcements of wing walls, HD13 and HD10 with the yield strength of 400 MPa were used for the main bars and the stirrups of wing wall, respectively.

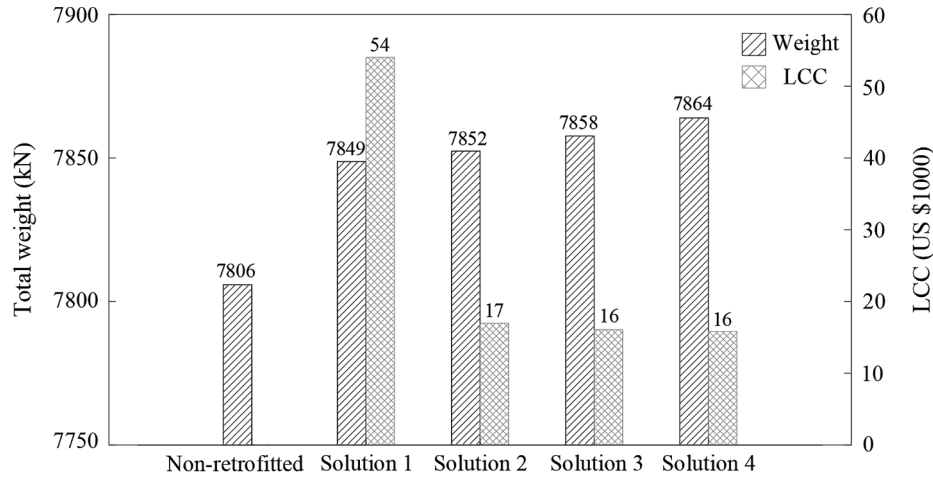


Fig. 13. Comparison of objective function values among non-retrofitted structure and 4 Pareto solutions for the six-storey RC office building.

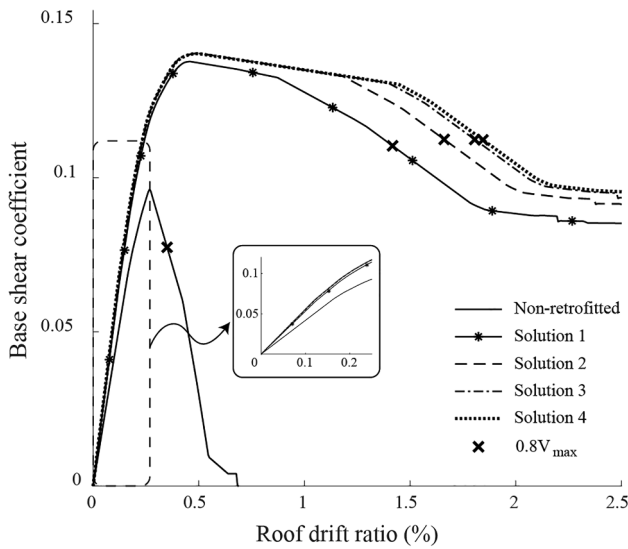


Fig. 14. Pushover curves of the non-retrofitted six-storey RC office building and each solution.

### 3.3. Constraint functions

In order to evaluate the seismic performance of a structure both before and after retrofitting, pushover analysis of FEMA356[43] was used. The example building used in this study was office and neighborhood facilities and the basic safety objective (BSO), which is a basic performance goal, was set as the performance goal. In order to satisfy the BSO performance goal, the structure must have sufficient seismic performance against the earthquakes of return period 474 years and 2,475 years. In FEMA 356, the limit value of inter-storey drift ratio (LS : 2%, CP: 4%) is suggested as an indicator of satisfying seismic performance. Therefore, we set this as the constraint function, which is shown in Eq. (9).

$$\text{Constraint } C_1 = \frac{\Delta_{\max, i \text{ level}}}{\Delta_{a, i \text{ level}}} \leq 1.0 \quad (9)$$

Here,  $i$  level represents the life safety (LS) level and collapse prevention (CP) level,  $\Delta_{\max}$  is the maximum storey drift ratio of a structure at each level, and  $\Delta_a$  is the permissible storey drift ratio of each level. In order to satisfy the BSO, the seismic performance of the structure must meet the LS level for the earthquake of the return period of 474 years. This means that the maximum inter-storey drift ratio of the structure in the event of the earthquake must be within 2% of the permissible inter-

storey drift ratio. For the earthquake of return period 2,475 years, the seismic performance of the structure should satisfy CP level, which means that the maximum inter-storey drift ratio of the structure should be within 4% of the permissible inter-storey drift ratio during the earthquake.

Structures retrofitted by wing walls may have shear failure depending on the section details of the wing wall. To prevent shear failure, the constraint function using the ratio in Eq. (1) was given by

$$\text{Constraint } C_2 = \frac{Q_{su}}{Q_{mu}} > 1.0 \quad (10)$$

The ratio in Eq. (10), was set to exceed 1.0. Thus, the section of the wing wall was set to have a bending failure for a retrofitted column.

Eq. (11) is a constraint function considering storey collapse prevention at CP level. The ultimate state is defined as the point where the maximum storey shear force is reduced by 20% (80% of the maximum storey shear force), and it is assumed that storey collapse occurs from this point. Therefore, the storey shear force value at CP level is set to be greater than 80% of the maximum storey shear force of the corresponding storey.

$$\text{Constraint } C_3 = \frac{i SF_{CP \text{ level}}}{i SF_{\text{storey failure}}} > 1.0 \quad (11)$$

$i SF_{CP \text{ level}}$  is the storey shear force of  $i^{\text{th}}$  storey on the CP level and  $i SF_{\text{storey failure}}$  is the 80% value of the maximum storey shear force of  $i^{\text{th}}$  storey.

Finally, as given in Eq. (12), in order to ensure constructability during retrofitting, both length  $lw_{(i+1)j}$  and thickness  $tw_{(i+1)j}$  of the wing wall for the column at the  $(i+1)$ -th floor were set to equal to or less than the length  $lw_{ij}$  and thickness  $tw_{ij}$  of the wing wall for the column at the  $i$ -th floor, respectively.

$$\text{Constraint } C_4 = lw_{ij} \geq lw_{(i+1)j} \text{ and } tw_{ij} \geq tw_{(i+1)j} \quad (12)$$

### 3.4. Solution process

In this paper, NSGA-II (Nondominated sorting genetic algorithm-II) [24] is used to determine an optimal retrofit solution for the purpose of minimizing the retrofit weight and LCC. If necessary, a random number generator is used to generate a population within the range of the design variables set in Section 3.2. Each individual of the population for NSGA-II has information of a different wing wall, including retrofit points, length and thickness of wing wall, and the amount of re-bar.

In order to apply the retrofitting method proposed in this paper, the seismic capacity of the existing building should be identified by the nonlinear static analysis first. To do this, we set up the non-linear parameters of the hinges on both sides of the element by evaluating the

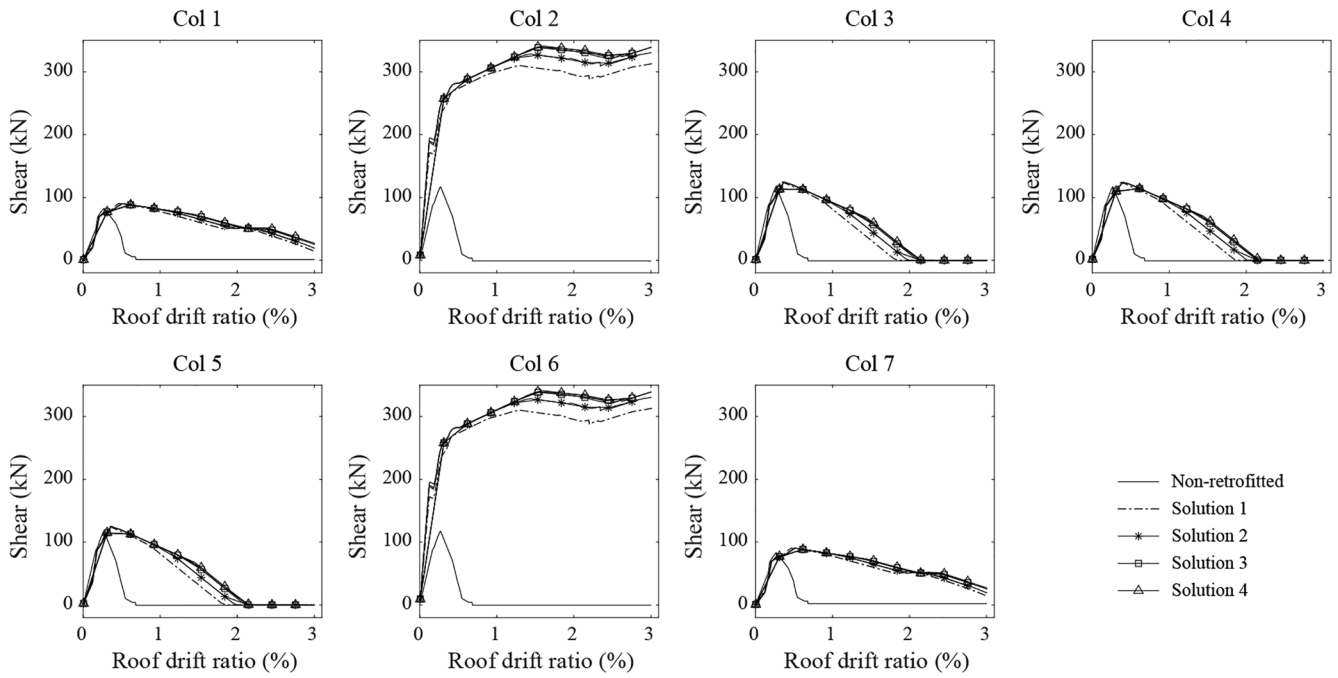


Fig. 15. Shear force according to roof drift ratio of the 1st floor columns of the 6-storey building example.

**Table 6**  
Dissipated energy of the non-retrofitted six-storey RC office building and each solution.

	Non-retrofitted	Solution 1	Solution 2	Solution 3	Solution 4
Dissipated energy (kN-m)	30.22	233.33	285.22	312.66	320.06
Dissipated energy ratio	-	7.72	9.44	10.35	10.59

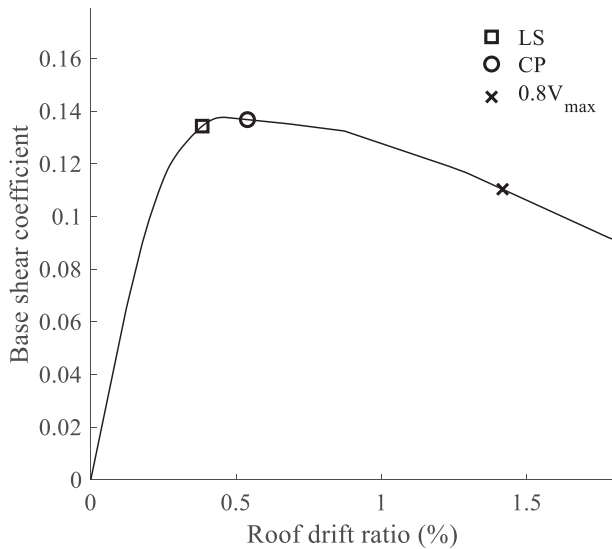


Fig. 16. Pushover curves of Solution 1 for the six-storey RC office building.

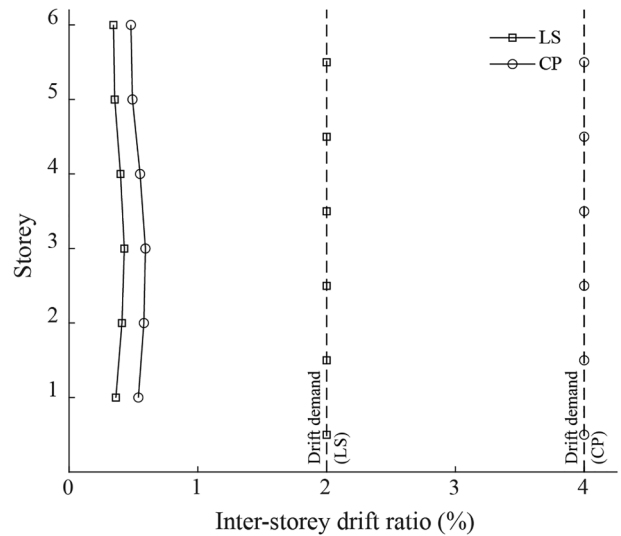


Fig. 17. Storey drift ratios of Solution 1 for the six-storey RC office building.

strength and failure modes of the members, as shown in Section 2.1, and modeling them using Opensees. The vertical distribution of the pseudo lateral load applied with the vertical distribution factor  $C_{vx}$  presented in FEMA356 was used for the lateral force distribution for the pushover analysis (Eq. (13)).

$$C_{vx} = \frac{w_x h_x^k}{\sum_{i=1}^n w_i h_i^k} \quad (13)$$

where,  $w_i$  and  $w_x$  are portion of the total building weight  $W$  located on or assigned to floor level  $i$  and  $x$ , respectively. And  $h_i$  and  $h_x$  are height from the base to floor level  $i$  and  $x$ , respectively.  $k$  is linear interpolation shall be used to calculate values of  $k$  for intermediate values of  $T$  ( $k = 2.0$  for  $T \geq 2.5$  seconds and  $k = 1.0$  for  $T \geq 0.5$  seconds).

In this study, displacement coefficient methods (DCM), one of the representative nonlinear static procedures proposed by FEMA356, were applied to evaluate the seismic performance before and after retrofitting of the building. As for the numerical analysis method, Newton algorithm (updates tangent stiffness at every iteration) provided by

**Table 7**  
Wing wall sections of Solution 1 for the six-storey RC office building.

	Wing wall	Col 1	Col 2	Col 3	Col 4	Col 5	Col 6	Col 7
Storey 1	Length (mm)	0	270	0	0	0	270	0
	Thickness (mm)	0	150	0	0	0	150	0
	Steel ratio (%)	0	0.75	0	0	0	0.75	0
Storey 2	Length (mm)	0	270	0	0	0	270	0
	Thickness (mm)	0	150	0	0	0	150	0
	Steel ratio (%)	0	0.75	0	0	0	0.75	0
Storey 3	Length (mm)	0	260	0	0	0	260	0
	Thickness (mm)	0	140	0	0	0	140	0
	Steel ratio (%)	0	0.75	0	0	0	0.75	0
Storey 4	Length (mm)	0	240	0	0	0	240	0
	Thickness (mm)	0	140	0	0	0	140	0
	Steel ratio (%)	0	0.75	0	0	0	0.75	0
Storey 5	Length (mm)	0	210	0	0	0	210	0
	Thickness (mm)	0	120	0	0	0	120	0
	Steel ratio (%)	0	0.75	0	0	0	0.75	0
Storey 6	Length (mm)	0	0	0	0	0	0	0
	Thickness (mm)	0	0	0	0	0	0	0
	Steel ratio (%)	0	0	0	0	0	0	0

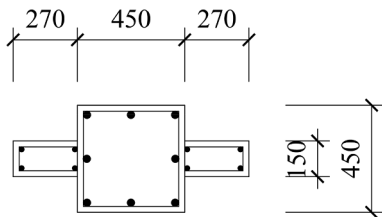


**Fig. 18.** Plan of Col<sub>12</sub> in Solution 1 for the six-storey RC office building.

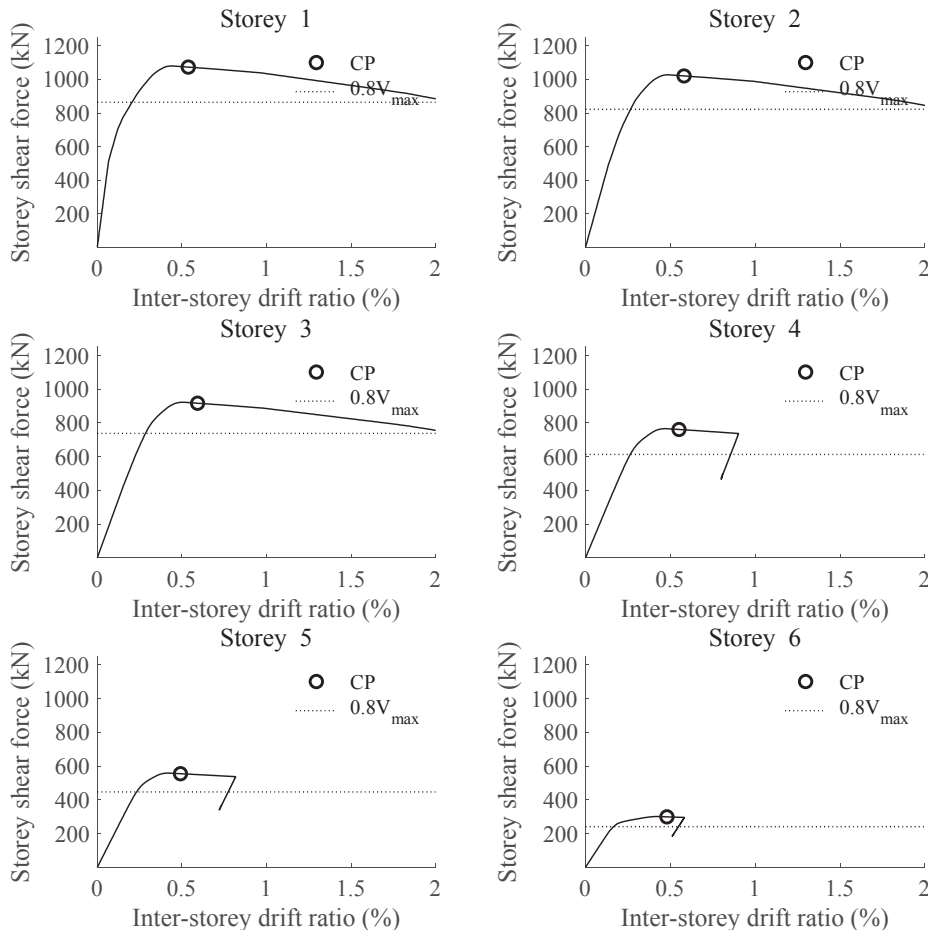
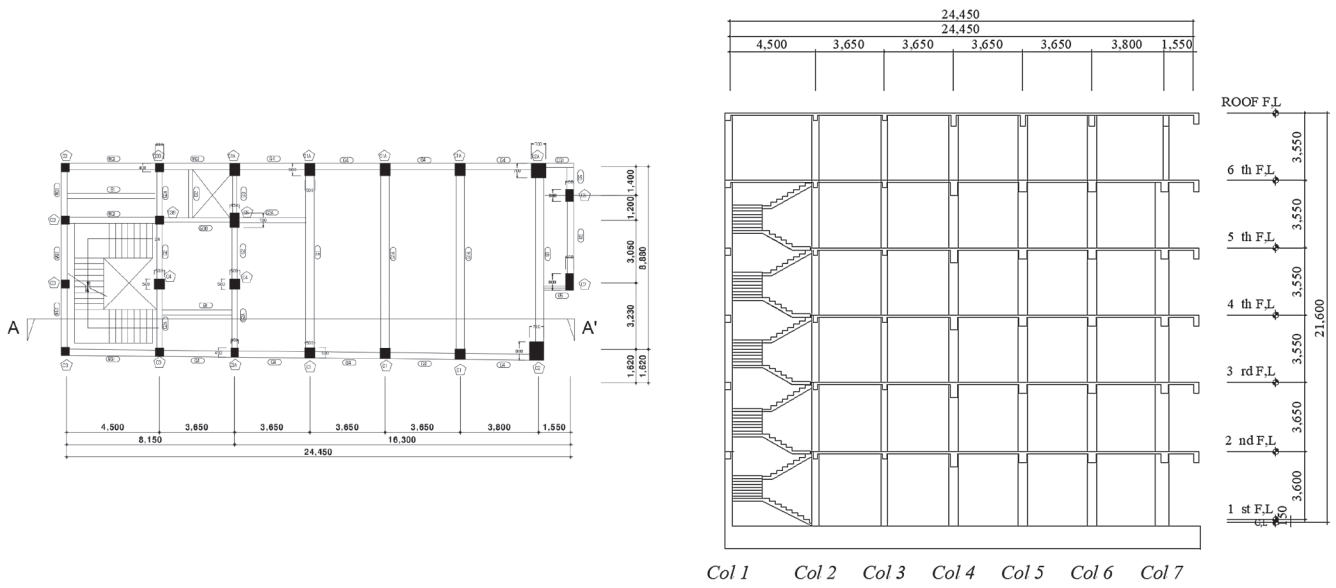


**Fig. 19.** Storey failure of Solution 1 in CP level for the six-storey RC office building.

OpenSees was used to determine the sequence of steps taken to solve the nonlinear equation. For the convergence criteria for the solution of unbalanced forces in nonlinear analysis,  $\sqrt{\Delta U^T \Delta U} < tol (tol = 10^{-5})$  of Norm displacement increment test (from OpenSees) was used to perform the analysis.

For the retrofitting target building, NSGA-II is used to find the retrofitting scheme optimized for the objective functions (Eqs. (4) and (5)) while satisfying the constraint functions (Eqs. (9)–(12)), in this process, the seismic performance of the retrofitted building is also evaluated through a nonlinear static procedure (i.e., DCM) for the numerical model that reflects the nonlinear hysteretic characteristics of the newly installed wing walls

Fig. 4 shows the numerical model of the building before retrofitting and the numerical model of the optimization process by NSGA-II. In the optimization process, one retrofitting scheme becomes one population, and the number of strings constituting the population is the total number of internal columns in which wing walls can be installed. A number is randomly assigned to each string starting from 1, where there is no retrofitting as in Fig. 4(1), to one number from the total number of wing wall sections that can be derived from the combination of design variables set in Section 3.2. In Fig. 4, when X1 to X3 are the columns in which the wing walls can be installed, the number of strings is three, and all string information is one for a building before retrofitting, such as Fig. 4(1). A random number is assigned to the string of initial populations, when number 9 is assigned to X2 as in Fig. 4(2), the hysteresis curve calculated based on the cross section information of the wing walls of number 9 is entered at both hinges of column X2. In addition, the beam around the X2 affected by the installation of the wing walls is changed to the rigid zone by the length corresponding to



(1) Plan of the standard floor of the actual building

(2) Section A-A'

Fig. 20. Floor plan of the 3rd floor and section A-A' of the actual building.

the wing walls width and the nonlinear hysteresis input to the hinge of the beam is recalculated considering the reduced beam length.

The numerical model reflecting the information of the string is used to determine the performance of the retrofitted building through the nonlinear static analysis and to calculate the satisfaction of the constraint functions and the objective functions. Based on the calculated values, the fitness for the objective function is evaluated, and each population is ranked according to the fitness evaluation results as shown in Fig. 5 as an example. Higher populations are selected and the information is passed on to the next generation, while lower ranking populations are eliminated. In addition, for the diversity of the solution,

generations are made that include populations that cross over populations during evolution and mutations. If the generated generation meets the stopping criteria set by the user, the genetic algorithm is terminated, and the population at this time becomes the pareto optimal solution. In this study, under the condition that the minimum number of households is more than 100, it is set to end when the number of households whose change rate of non-governing solution is 3% or less is more than 300 consecutive generations or when the number of generations reaches 3000. The above optimization process is represented by a flow chart (Fig. 6), and the details of NSGA-II used in this study can be found in [34].

Table 8  
Detailed sections of columns of the actual building example

Column	Col <sub>11</sub> ~ Col <sub>61</sub> Col <sub>12</sub> ~ Col <sub>62</sub>	Col <sub>13</sub> ~ Col <sub>33</sub>	Col <sub>43</sub> ~ Col <sub>63</sub>	Col <sub>14</sub> ~ Col <sub>14</sub> , Col <sub>15</sub> ~ Col <sub>45</sub> , Col <sub>16</sub> ~ Col <sub>46</sub>	Col <sub>54</sub> , Col <sub>55</sub> Col <sub>56</sub>
Section					
Re-bar	6-D19	8-D25	8-D19	10-D25	10-D19
Stirrup	D10@200	D10@200	D10@200	D10@200	D10@300
Column	Col <sub>64</sub> , Col <sub>65</sub> Col <sub>66</sub>	Col <sub>17</sub> ~ Col <sub>37</sub>	Col <sub>47</sub>	Col <sub>57</sub>	Col <sub>67</sub>
Section					
Re-bar	10-D19	8-D25	8-D19	8-D19	8-D19
Stirrup	D10@300	D10@300	D10@300	D10@300	D10@300

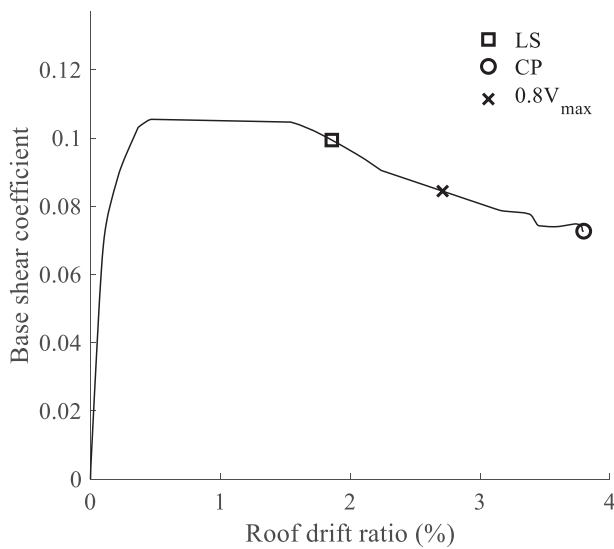


Fig. 21. Pushover curves of the actual building.

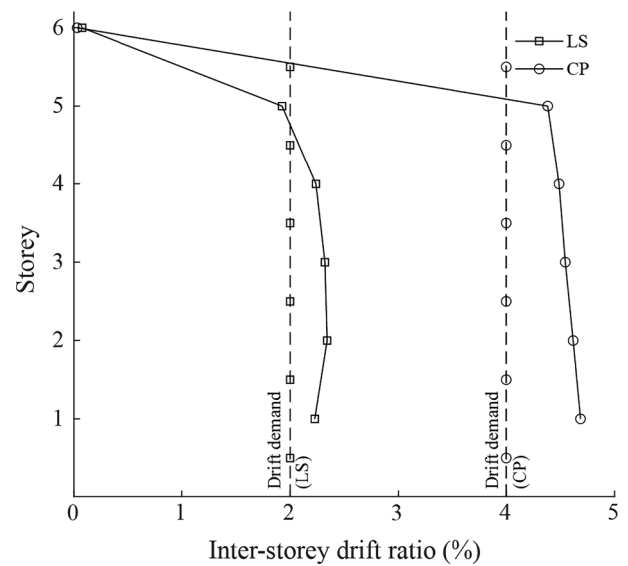


Fig. 22. Inter-storey drift ratios of the actual building.

## 4. Applications to seismic retrofit

### 4.1. Six-storey office building

#### 4.1.1. Overview

As a seismic retrofit method to improve the lack of flexural strength and deformation capacity due to shear failure, which are structural features of buildings that do not meet the current seismic design criteria, wing wall retrofitting can be used. Also in this study, the applicability of the optimal seismic retrofit technique by the wing wall (improved flexural/shear strength and deformation capacity enhancement) was examined by selecting a building whose columns represent shear failure mode from RC frame buildings without seismic design to improve seismic performance through wing wall retrofitting.

For the purpose of verification, the proposed method was applied to a six-storey RC structure for an office building, which was used by AE Ozel and EM Guneyisi [13]. The structure was constructed in 1975 according to the Turkish seismic standard [45]. However, as the performance of the structure was evaluated by the displacement coefficient method of FEMA 356, San Francisco, USA and the soil grade D (stiff soil) were assumed as the region and soil information, respectively. Fig. 7 shows the plan and elevation of the structure. The structure was designed as an office building. Columns were named based on Fig. 3. Table 2 presents sectional details. The structure was symmetrical with respect to center line.

In this paper, only structural members are considered dead loads to estimate the axial force of vertical members. For live load,  $2 \text{ kN/m}^2$  was applied in the same way as the original paper (AE Ozel [13]) for the tributary area of members. The base of the columns at the ground floor was analyzed as having a fixed end.

The concrete compressive strength used for columns and beams was 16 MPa, and the yield strength of reinforcement was 220 MPa (AE Ozel [13]).

To identify the nonlinear behavior of the building before retrofitting, the ratio in Eq. (1) was calculated. The behaviors of the columns at failure can be found using the ratio in Table 3. As can be seen in Table 3, this six-storey RC office building showed a shear failure at all the columns of the 1st storey and the inner columns of the 2nd and 3rd stories. The remaining columns and beams showed flexural failure since the constraint in Eq. (10) was satisfied (Table 3, 4). When the seismic performance was identified by the nonlinear static analysis, the pushover curves of Fig. 8 could be obtained. In Fig. 8, roof drift ratio is the ratio of lateral displacement at roof to total height of a building (18 m),

and base shear coefficient is the ratio of base shear force to total weight of a building (7805.8 kN). As can be seen in Fig. 8, the roof drift ratio of LS level was 0.59%. This was less than the ultimate drift (0.35%), which indicates the drift at the point where the maximum base shear dropped by 20%. The behavior in CP level could not be evaluated because the building strength became 0 before reaching the performance point. Accordingly, the storey drift ratio and storey failure of the structure could be identified in LS level. Fig. 9 illustrates the storey drift ratios of the structure in LS level. The maximum inter-storey drift ratio was 3.35% on the 3rd floor, where the size of the column section changed.

The relationship between storey shear force and inter-storey drift ratio of the example in LS level is shown in Fig. 10. As shown in Fig. 10, regarding the story collapse, the shear forces were much smaller than 80% of the maximum strength, which was assumed to be the point of story collapse. Consequently, this RC building example did not satisfy the story drift ratio of 2%, i.e., the criterion for LS level in the BSO, which was set as the target seismic performance. Besides, the story collapse already occurred in LS level as can be seen in Fig. 10.

As in Fig. 10, the strength decrease occurs in the 3rd storey column where the cross section of the column decreases, which indicates that the 3rd storey upper and lower columns are in unloading state to satisfy the equilibrium conditions of forces at the joints (nodes) with adjacent storey members. The load used in the pushover analysis is a monotonically increasing form, but the hysteretic model applied to the both ends of the hinges of the members has rules of hysteretic behaviours along with a skeleton curve. Therefore, the hysteresis curve showing the load-displacement relationship follows the rules of hysteretic behaviours of loading, unloading, and reloading, not the shape moving on the skeletal curve. Therefore, as in Fig. 10, the hysteric shape of unloading is shown in the force-displacement relationship for storeys other than 3rd storey.

#### 4.1.2. Optimal retrofit solution

The building was retrofitted by the proposed method. To ensure retrofitting efficiency, Col 2, Col 4, and Col 6 were considered for the retrofit design during optimization. In addition, to enhance constructability, the columns were symmetrically retrofitted with respect to Col 4, which was center line. Fig. 11 shows the evolution of each generation by applying the multi-purpose genetic algorithm to the example building. Fig. 11(1) and Fig. 12(2) show only the minimum values of the objective function values of the populations that constitute a generation. For the example, the evaluation ended at 1333 generation by

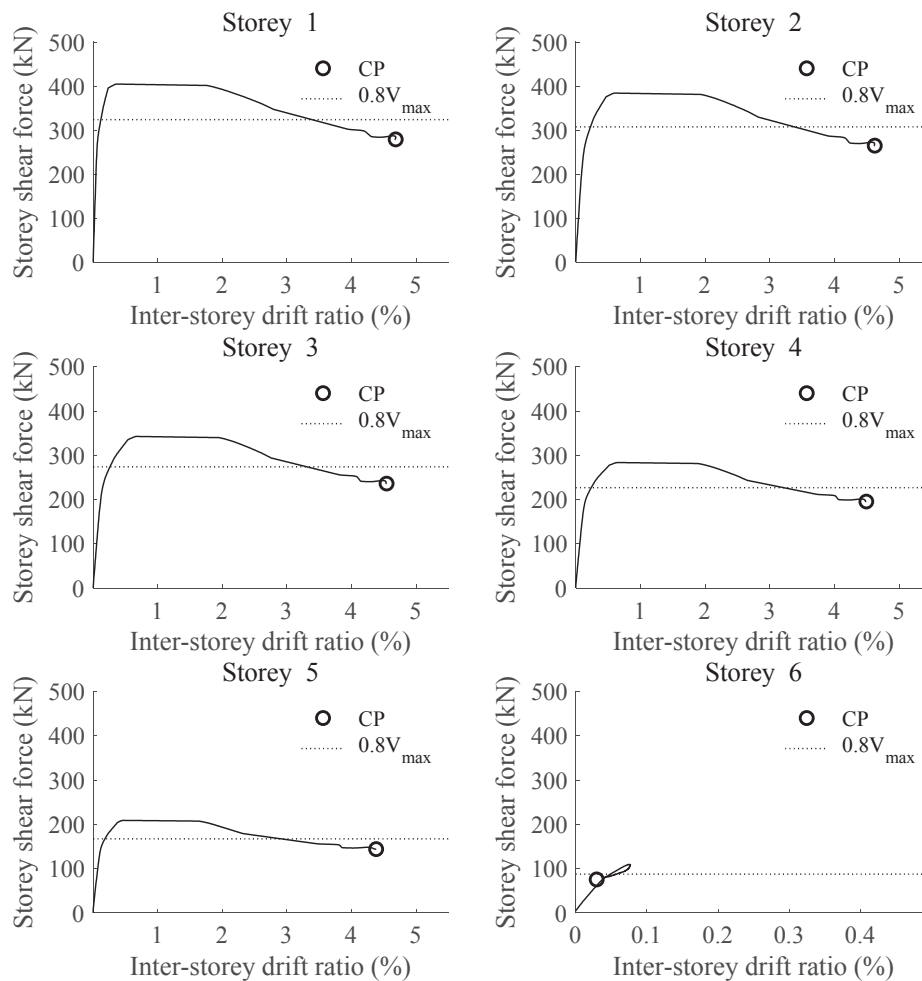


Fig. 23. Storey failure of the actual RC building in CP level.

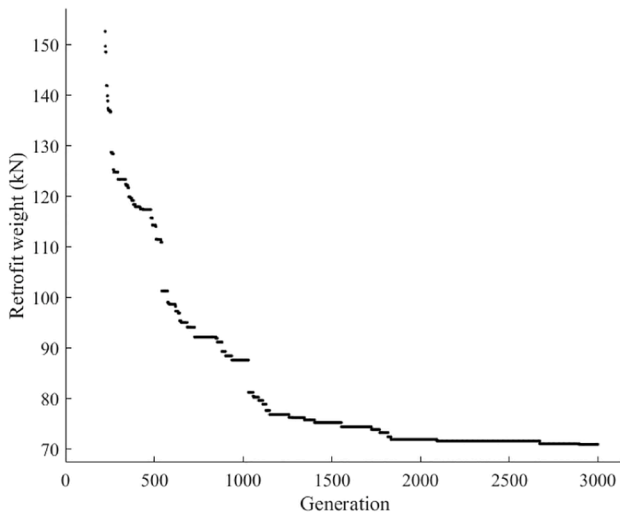
the set stopping criteria set in Section 3.4. The appropriateness of the solution convergence for each objective function can also be confirmed by Fig. 11(3), which shows the Pareto solution for each generation. Among the Pareto solutions of the last generation, Solution 1 and Solution 4 in Fig. 11(3) represent optimal retrofit designs for the minimization of retrofit weight and the minimization of LCC, respectively. Solution 2 was selected based on the minimum value among the sums of the objective function values of each Pareto solution divided by the minimum values of retrofit weight and LCC, respectively. Solution 3 was randomly selected from the solutions for comparison. As shown in Fig. 12(1), the retrofiting positions of the solutions were all identical, and the 2nd column and 6th column columns were symmetrically retrofitted based on C.L from 1st to 5th floor. The shapes of columns with retrofitted wing walls from Solutions 1 to 4 were different shapes, as shown in Fig. 12(2)–(4), and the steel ratios of the wing walls were also different.

The hinge parameters for considering the nonlinear characteristics of the beam were also calculated based on the method proposed in FEMA356. When the failure mode of the beam of the building before the retrofiting was determined through the strength formula, all beams were evaluated as flexural failure mode (Table 4). After retrofiting, the clear length of the beam is reduced because the length corresponding to the width of the wing wall constrains the beam. Thus, the failure mode is expected to change because the shear force for bending strength increases. Therefore, after retrofiting, the failure mode was re-evaluated in consideration of the shortened beam length, and shear failure did not occur in the beam even after retrofiting (Table 5).

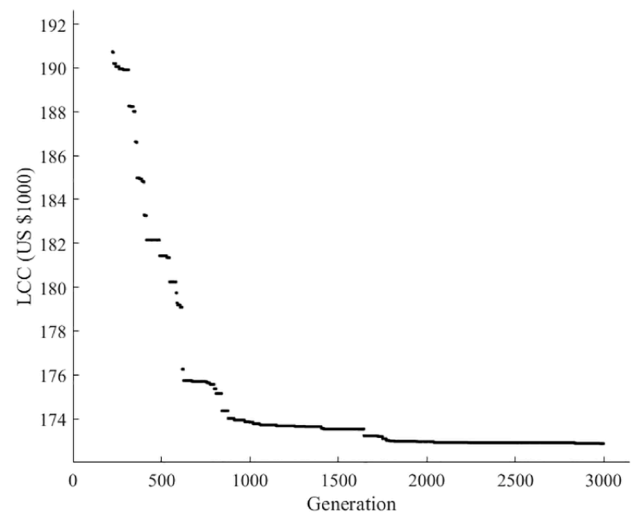
Fig. 13 presents the total weights and LCCs required by non-retrofitted structure and each solution. Before retrofitting, the building had a total weight of 7805.87 kN. Solution 1, which was optimized to minimize the retrofit weight, achieved target seismic performance with a retrofit weight of 42.88 kN, which corresponds to 0.55% of the weight of the non-retrofitted building. For this example, LCC for the non-retrofitted building could not be evaluated in CP level due to lack of seismic capacity. However, Solution 4 required an LCC of only \$15,830 for the life cycle of the building. This was 29.3% of \$54,030, which was the LCC required by Solution 1.

Fig. 14 shows the pushover curves of each solution and the non-retrofitted building. The comparison of non-retrofitted and retrofitted buildings shows that the maximum shear force is improved by about 40%, but the increase in initial stiffness is not significant. Significant increase in deformation capacity in retrofitted buildings is the result of improving strength degradation in the existing columns by wing wall retrofiting. It is considered that the reason for no significant difference in the initial stiffness between the non-retrofitted and retrofitted buildings is that the increase in cross-sectional secondary moment due to the increase in wing wall width is not large enough to significantly increase the stiffness of the whole building.

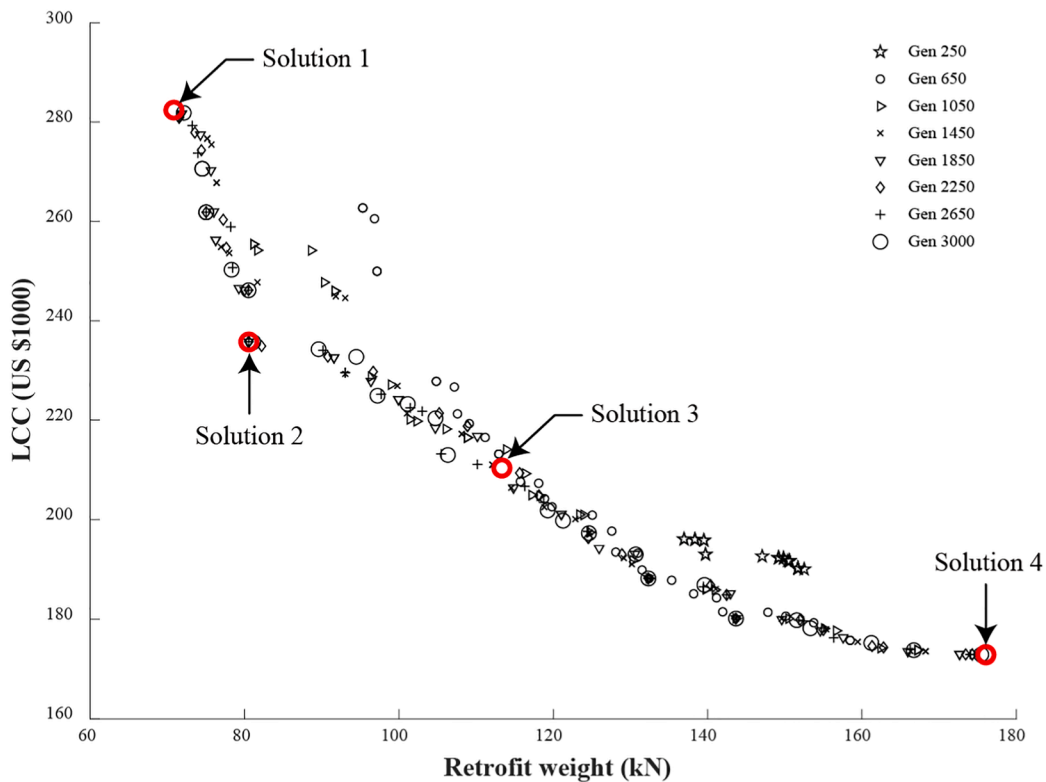
On the other hand, it can be seen that there is no significant difference in the performance curve of retrofitting solutions because the location and quantity of wing walls are the same in the retrofitted building and there are slight differences in thickness and width (Fig. 12). Fig. 15 shows the first-storey column shear forces of the four solutions before and after retrofiting, indicating that there is no



(1) Convergence curve for retrofit weight



(2) Convergence curve for LCC



(3) Pareto solutions by generation

Fig. 24. The evolution process of NSGA-II.

significant difference in the hysteresis curves of the individual columns.

Each pushover curve displays a point corresponding to 80% of the maximum base shear, where the load-carrying capacity is regarded as being lost. In addition, the area under each pushover curve until the point, i.e., 80% of the maximum base shear, can be considered as the energy dissipation capacity indicating the ability of the structure. The accurate evaluation of dissipated energy requires cyclic static analyse or non-linear time history analyses, but this paper is aimed to compare the retrofitting effect of optimized solutions (retrofitted buildings) by calculating the area under the pushover curve. Table 6 presents the dissipated energy values of each solution [5,44]. The dissipated energy of the non-retrofitted building was 30.22 kN·m. Solution 1, which required the minimum retrofit weight among the Pareto solutions, had a

dissipated energy of 233.33 kN·m. This was 7.72 times that of the non-retrofitted building. Thus, the proposed retrofit method using wing wall could improve the seismic performance of the building.

Fig. 16 shows the pushover curves of Solution 1, which was optimized to minimize the retrofit weight. The CP level of non-retrofitted structure could not be evaluated due to lack of strength before retrofitting. However, after the structure was retrofitted, the drift values of every level were less than the ultimate drift. In addition, as shown in Fig. 17, the inter-storey drift ratios at each performance point were 0.43% in LS level and 0.59% in CP level, which satisfies the target seismic performances for LS level (2%) and CP level (4%), respectively. Thus, the retrofitted building showed sufficient seismic performance. Table 7 presents the wing wall sections and the steel ratios of Solution

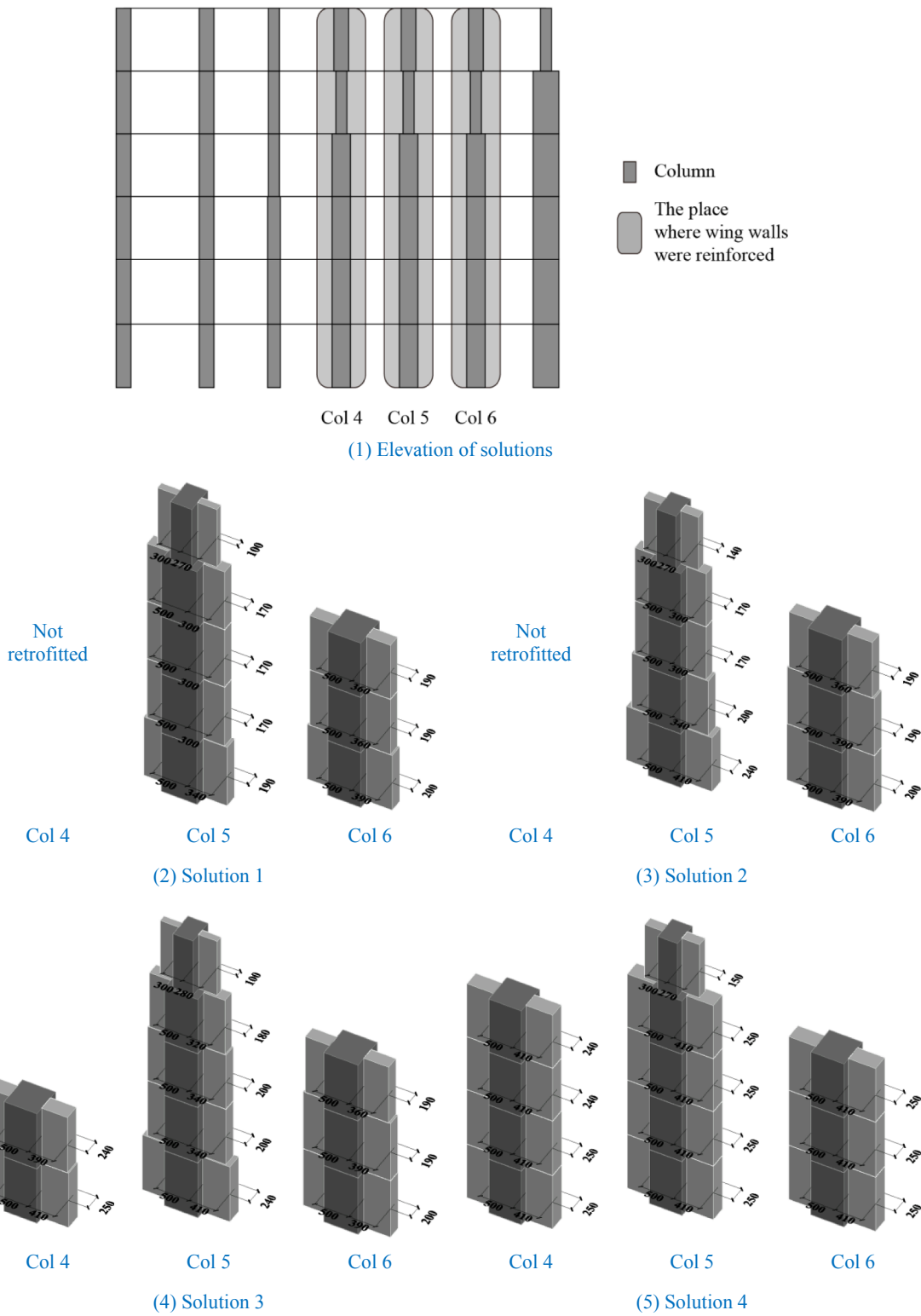


Fig. 25. The shape of Pareto solutions of the actual building example.

1. Fig. 18 illustrates the section of Col<sub>12</sub>, which was the retrofitted Col 2 at the 1st floor in Table 7.

The relationship between storey shear force and inter-storey drift ratio of Solution 1 in CP level is shown in Fig. 19. In Fig. 19, although there is no sudden decrease in strength and concentration of drift, the hysteresis of unloading is observed in the 4th, 5th, and 6th stories. This is a result to satisfy the equilibrium conditions at the nodes due to

nonlinear behavior. While the non-retrofitted building underwent a storey collapse in LS level due to a drastic decrease of strength or the lack of member strength, all stories of the retrofitted one had a storey strength 1.24 times larger than the storey collapse criterion in CP level, so it did not show any storey collapse, as illustrated in Fig. 19. Thus, Solution 1 with the minimum retrofit weight achieved a sufficient improvement of seismic performance.

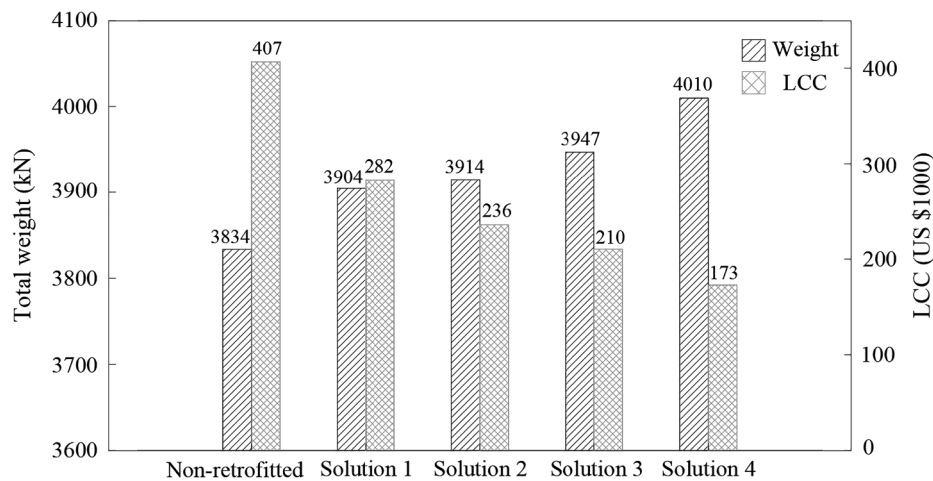


Fig. 26. Comparison of objective function values among non-retrofitted structure and 4 Pareto solutions for the actual building example.

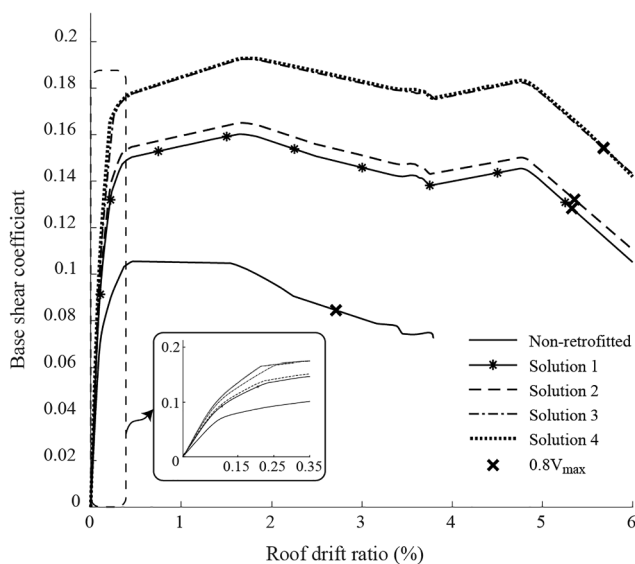


Fig. 27. Pushover curves of the non-retrofitted actual building and each solution.

#### 4.2. Seismic retrofit of actual six-storey six-span RC frame structure

##### 4.2.1. Overview

The proposed method in this study was applied to seismic retrofit design of an actual building in use. The building is a six-story six-span RC structure constructed in the 1920 s in Korea. The floor plan and section view of the building is shown in Fig. 20. The compressive strength of concrete and yield strength of re-bars used in the building were 20 MPa and 240 MPa, respectively, which were the design strength at the time of building design. As rigid diaphragms were used to connect vertical members in each floor of this building, the section A-A' was analyzed. The base of the columns at the ground floor was analyzed as having a fixed end. The dead load used in the analysis only considers the self-load of structural members, and the live load is set as  $3kN/m^2$  in consideration of the neighboring living facility that is the purpose of the building. Table 8 presents the information of columns for the section A-A'. Base on the nonlinear analysis of the building before the retrofit, it was found that Col 4, Col 5, and Col 6 at the 1st to 3rd stories showed shear failure and the remaining members had flexural failure.

The pushover curve for the building before the retrofit obtained by nonlinear static analysis of FEMA356 is given in Fig. 21. As shown in

Fig. 21, the roof drift ratio in CP level was 3.80%, which was larger than the ultimate drift ratio (2.71%). Fig. 22 illustrates the inter-storey drift ratios in each performance level on the pushover curves. The building had the storey drift ratios of 2.34% in LS level and 4.69% in CP level. The relationship between storey shear force and inter-storey drift ratio of the example in CP level is shown in Fig. 23. In CP level, the strength of each floor was less than 80% of the maximum strength, which was set as the criterion of storey collapse, as shown in Fig. 23. As the building did not satisfy the permissible storey drift ratio in both LS and CP levels and showed a storey collapse in CP level, it was retrofitted by the proposed method of this study. In the case of this building, since it was impossible to add wing walls to Col 1, and Col 2, Col 3 due to the existing masonry walls, Col 4, Col 5, and Col 6 were selected to be retrofitted by wing walls. These columns had the largest tributary area among the inner columns and showed partial shear failure.

##### 4.2.2. Results

By applying the technique proposed in this study to the real-structure example, we could obtain the evolutionary picture by generation such as Fig. 24. Fig. 24(1) and (2), which are retrofit weight and convergence curve for LCC set as the objective function of the method show only the minimum values of the objective function values of the populations of one generation. The evolution ended at 3000 generation set as the stopping criteria for the real building example. Fig. 24(3) also shows that as generations evolve, populations converge on the objective function. Among the Pareto solutions of the last generation, Solution 1 was optimized to minimize the initial retrofit weight. Solution 2 was selected based on the minimum value among the sums of the objective function values of each Pareto solution divided by the minimum values of retrofit weight and LCC, respectively. Solution 3 was randomly selected among the solutions that adequately satisfied any two objective functions. Solution 4 was related to the minimization of LCC. The retrofitting shape of each solution is as shown in Fig. 25., and Fig. 26. presents the total weights and LCCs for non-retrofitted structure and each solution. Before retrofitting, the building had a total weight of 3833.6 kN. Solution 1, which was optimized to minimize the retrofit weight, achieved the target seismic performance with the retrofit weight of 70.85 kN, which corresponds to 1.85% of the weight of the non-retrofitted building. On the other hand, Solution 4 required an LCC of \$172,870 for the life cycle of the building. This was 42.52% of \$406,530, which was required by the non-retrofitted building.

In order to compare seismic responses of the non-retrofitted building and the retrofit solutions from the proposed method, pushover curves for the initial building and 4 solutions are presented in Fig. 27. Each pushover curve displays a point corresponding to 80% of the maximum base shear, where the load-carrying capacity is regarded as being lost.

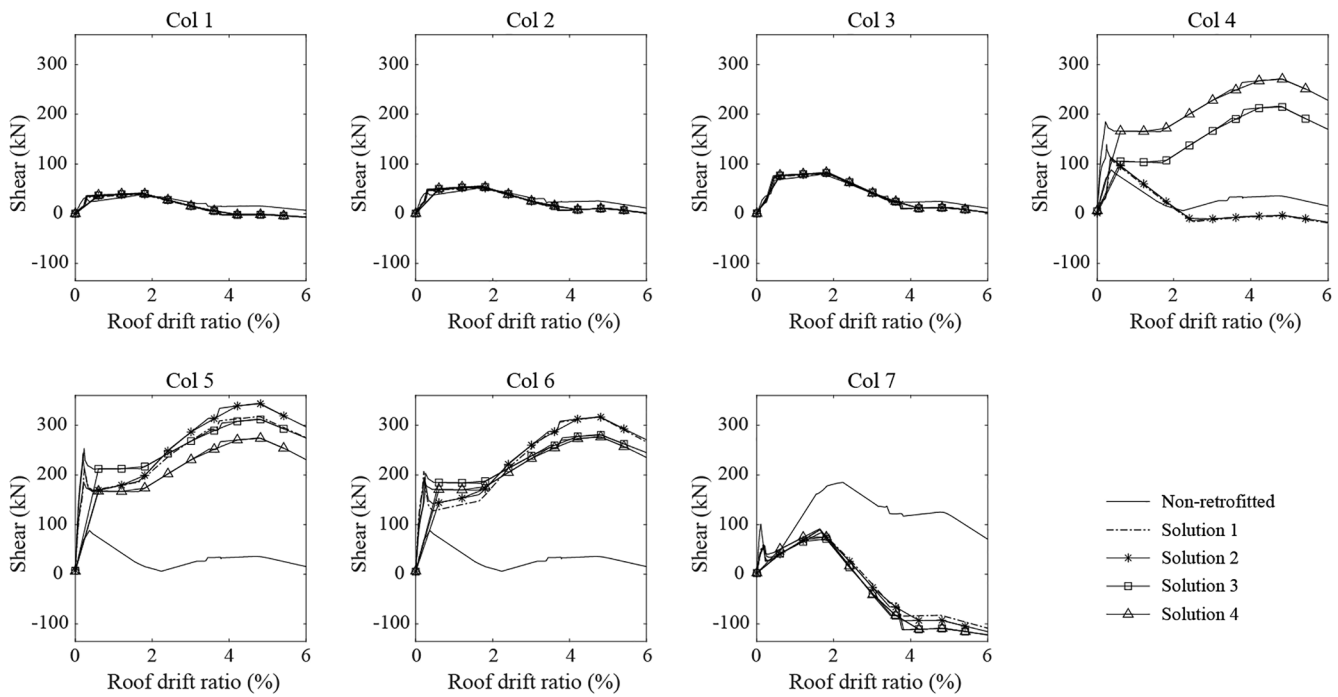


Fig. 28. Shear force according to roof drift ratio of the 1st floor columns of the 6-storey building example.

Table 9

Dissipated energy of the non-retrofitted actual building and each solution.

	Non- retrofitted	Solution 1	Solution 2	Solution 3	Solution 4
Dissipated energy (kNm)	214.65	647.35	673.49	852.13	870.05
Dissipated energy ratio	-	3.02	3.14	3.97	4.05

Table 10

Wing wall sections of Solution 1 for the actual building.

	Wing wall	Col 1	Col 2	Col 3	Col 4	Col 5	Col 6	Col 7
Storey 1	Length	0	0	0	0	340	390	0
	Thickness	0	0	0	0	190	200	0
	Steel ratio	0	0	0	0	1	1	0
Storey 2	Length	0	0	0	0	300	360	0
	Thickness	0	0	0	0	170	190	0
	Steel ratio	0	0	0	0	1	1	0
Storey 3	Length	0	0	0	0	300	360	0
	Thickness	0	0	0	0	170	190	0
	Steel ratio	0	0	0	0	1	1	0
Storey 4	Length	0	0	0	0	300	0	0
	Thickness	0	0	0	0	170	0	0
	Steel ratio	0	0	0	0	1	0	0
Storey 5	Length	0	0	0	0	270	0	0
	Thickness	0	0	0	0	100	0	0
	Steel ratio	0	0	0	0	0.75	0	0
Storey 6	Length	0	0	0	0	0	0	0
	Thickness	0	0	0	0	0	0	0
	Steel ratio	0	0	0	0	0	0	0

It can be seen that the shear force of the retrofitted solution is improved compared to the non-retrofitted building, and there is a difference in the maximum shear force between the retrofitted buildings depending on the solution. On the other hand, there is no significant difference in initial stiffness between non-retrofitted and retrofitted buildings, as in the example building in Chapter 4. Fig. 28 compares the changes in column shear forces on the first floor of non-retrofitted building and retrofitted solution. As a result of failure mode analysis before retrofitting, the columns 1, 2, and 3 showing the flexural failure mode showed no difference in shear force before and after retrofitting,

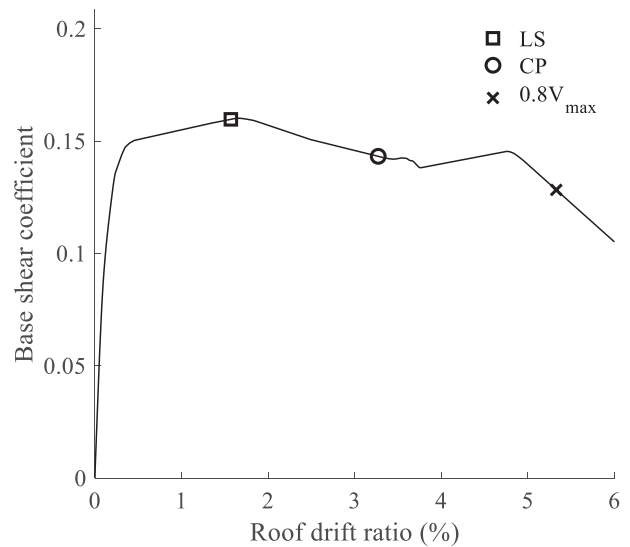


Fig. 29. Pushover curves of Solution 1 for the actual building.

because the retrofitting was not performed. On the other hand, as a result of comparing the column shear force after retrofitting, the columns 5 and 6, which have similar position and size of retrofitting of the wing-wall in all solutions, do not differ according to the solution. It can be seen that significant difference occurred in retrofitted column 4 only in solutions 3 and 4. Therefore, we can see that the difference in hysteresis curve for each retrofitted solution shown in Fig. 27 is due to the difference of retrofitting in column 4.

Table 9 presents the energy dissipation capacity, which indicates

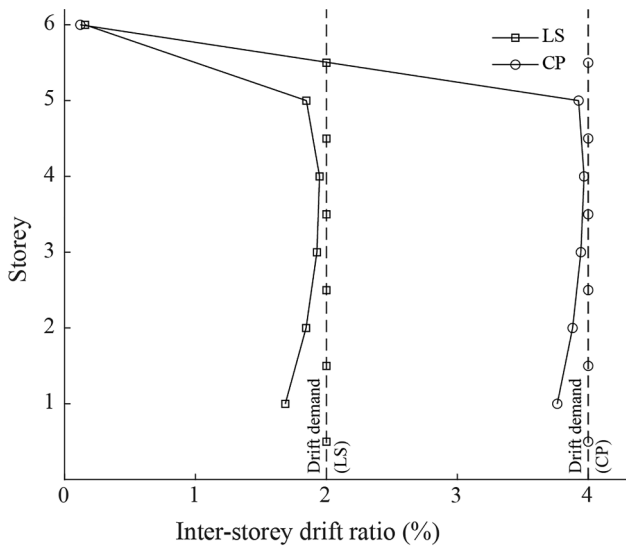


Fig. 30. Inter-storey drift ratios of Solution 1 for the actual building.

the ability of a structure to endure a seismic load. The dissipated energy of the non-retrofitted building was 214.65 kN-m. On the other hand, the retrofit solutions obtained by applying the proposed method increased

the energy dissipation capacity between 3.02 and 4.05 times compared to the non-retrofitted building. Thus, the seismic performance of the actual building was improved.

Table 10 presents information about wing wall sections of Solution 1, which required the minimum retrofit weight among the Pareto solutions. The nonlinear static analysis was conducted for Solution 1, and the pushover curves in Fig. 29 were obtained. Before retrofitting, as can be seen in Fig. 21, the drift value of the building in CP level was larger than the ultimate drift. However, after the building was retrofitted by wing walls, as shown in Fig. 29, the drift values of the performance point at every earthquake level were less than the ultimate drift. In addition, as shown in Fig. 30, the storey drift ratios at each performance point were 1.95% in LS level and 3.97% in CP level, thereby satisfying BSO, which was the target seismic performance. As illustrated in Fig. 31 for the relationship between storey shear force and inter-storey drift ratio of Solution 1 in CP level, no storey collapse occurred in CP level. Thus, it can be concluded that the desired seismic retrofit was achieved.

5. Conclusion

In this paper, an optimal retrofit design method for RC structure using wing walls is developed to improve the strength of columns and the ductility capacity of RC structures. To achieve the target seismic performance at the lowest possible cost, the retrofit weight was set as an objective function. In addition, to minimize the maintenance cost that may occur during the entire life cycle of a building, the LCC was

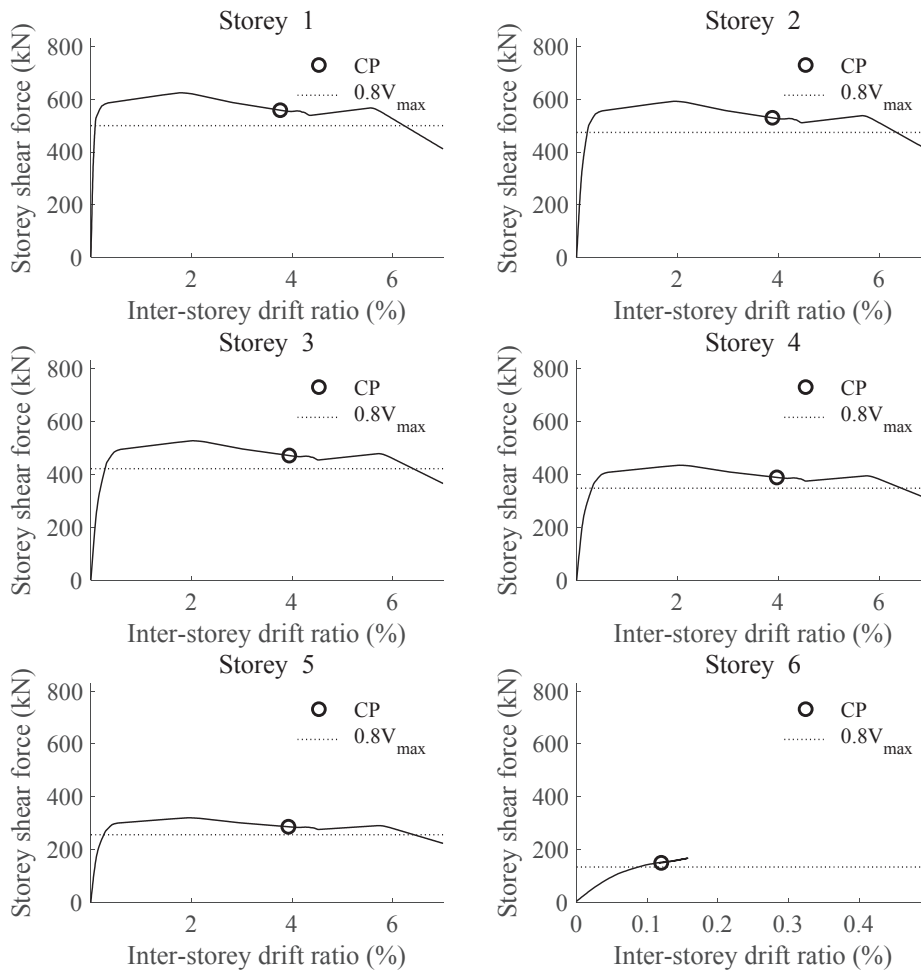


Fig. 31. Storey failure of Solution 1 in CP level for the actual building example.

also set as an objective function. The performance of the proposed retrofit design method was examined by application to seismic retrofit of a six-storey RC building example and an actual RC building structure in use. In order to verify the seismic performance of the retrofitted structure, pushover curves, the inter-storey drift ratios, the energy dissipation capacities, and failure modes of the non-retrofitted building and the retrofit solutions from the proposed method have been compared. Based on the comparison, it has been confirmed that, retrofit designs from the proposed method satisfied the target seismic performance and prevented storey collapse in CP level. In addition, the

relationship between the initial cost and LCC of retrofit designs have been presented for the selection of the most appropriate retrofit solution for each purpose or situation.

## Acknowledgments

This work was supported by a National Research Foundation of Korea (NRF) grant funded by the Korea government (MSIP) (No. 2011-0018360 and No. 2018R1A5A1025137).

## Appendix A

The calculation formula for the flexural yield strength of the column varies depending on the axial force acting and they are shown below.

$$\text{When } N_{\min} \leq N < 0, \quad M_y = 0.8A_s f_y D + 0.4ND \quad (\text{A1-a})$$

$$\text{When } 0 \leq N < N_b, \quad M_y = 0.8A_s f_y D + 0.5ND \left( 1 - \frac{N}{bDF_c} \right) \quad (\text{A1-b})$$

$$\text{When } N_b \leq N < N_{\max}, \quad M_y = (0.8A_s f_y D + 0.12bD^2 F_c) \left( \frac{N_{\max} - N}{N_{\max} - N_b} \right) \quad (\text{A1-1c})$$

where symbols used in Eq. (A1-a)–(A1-c) are given below.

$$N_{\min} = -A_s f_y - A_s' f_y$$

$$N_b = 0.4bDF_c$$

$$N_{\max} = bDF_c + A_s f_y + A_s' f_y$$

$N$ : axial force

$F_c$ : compressive strength of concrete ( $N/mm^2$ )

$f_y$ : yield strength of main reinforcement ( $N/mm^2$ )

$b$ : width of column

$D$ : depth of column

$A_s$ : cross area of tension reinforcement

$A_s'$ : cross area of compressive reinforcement

The shear yield strength of the column is given as follows.

$$Q_y = \left[ \frac{0.053p_t^{0.23}(F_c + 18)}{M/(Qd) + 0.12} + 0.85\sqrt{p_w \sigma_{wy}} + 0.1\sigma_0 \right] bj \quad (\text{A2})$$

where symbols used in Eq. (A2) are given below.

$p_t$ : tension reinforcement ratio (%)

$F_c$ : compressive strength of concrete ( $N/mm^2$ )

$M/(Qd)$ : shear span to depth (when  $M/(Qd) \leq 1$ ,  $M/(Qd) = 1$  and when  $M/(Qd) \geq 3$ ,  $M/(Qd) = 3$ )

$M/Q$ : shear span (also acceptable to calculated as half the length of column net length)

$d$ : effective depth of column.

$p_w$ : ratio of shear reinforcing bar (when  $p_w \geq 0.012$ ,  $p_w = 0.012$ )

$\sigma_{wy}$ : yield strength of shear reinforcing bar ( $N/mm^2$ )

$\sigma_0$ : Axial stress (if  $\sigma_0 > 8$ ,  $\sigma_0 = 8 N/mm^2$ )

$b$ : width of column

$j$ : Distance between the centers of stress (it is acceptable to set it as  $0.8D$ )

The flexural yield strength of the beam is as follows.

$$M_y = 0.8A_s f_y D \quad (\text{A3})$$

where symbols used in Eq. (A3) are given below.

$A_s$ : cross area of tension reinforcement

$f_y$ : yield strength of main reinforcement ( $N/mm^2$ )

$D$ : depth of beam

The shear yield strength of the beam is given below.

$$Q_y = \left[ \frac{0.053p_t^{0.23}(F_c + 18)}{M/(Qd) + 0.12} + 0.85\sqrt{p_w \sigma_{wy}} \right] bj \quad (\text{A4})$$

where symbols used in Eq. (A4) are given below.

$p_t$ : tension reinforcement ratio (%)

$F_c$ : compressive strength of concrete ( $N/mm^2$ )

$M/(Qd)$ : shear span to depth (when  $M/(Qd) \leq 1$ ,  $M/(Qd) = 1$  and when  $M/(Qd) \geq 3$ ,  $M/(Qd) = 3$ )

- e:shear span (also acceptable to calculated as half the length of column net length)
- d:effective depth of beam.
- $p_w$ : ratio of shear reinforcing bar (when  $p_w \geq 0.012$ ,  $p_w = 0.012$ )
- $\sigma_{wy}$ : yield strength of shear reinforcing bar ( $N/mm^2$ )
- b:width of beam
- j:Distance between the centers of stress (it is acceptable to set it as 0.8D)

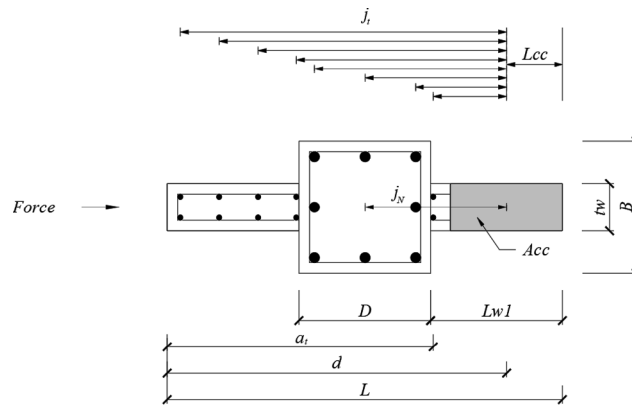
**Appendix B**

The flexural yield strength of the column with the retrofitting of the wing walls as in Eq. (2) is given below.

$$M_y = \sum (a_t \times \sigma_y \times j_t) + N \times j_N \tag{B1}$$

where symbols used in Eq. (B1) are given below.

- $a_t$ :cross area of tension reinforcement
- $\sigma_y$ : yield strength of tension reinforcement ( $N/mm^2$ )
- $j_t$ :distance between tension reinforcement and stress center of concrete compression area
- N:axial force
- $j_N$ :distance between action point of axial force and stress center of concrete compression area (see figure)



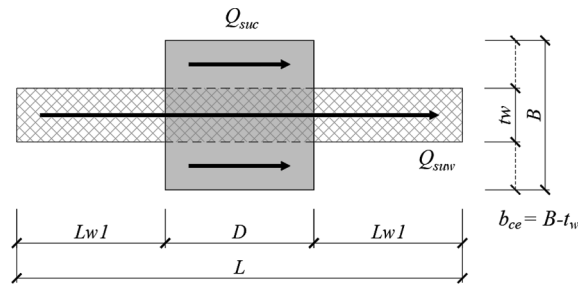
$A_{cc}$ :area of the concrete compression and can be calculated with the Eq. (B2) as below.

$$A_{cc} = \frac{\sum (a_t \times \sigma_y) + N}{\beta_{cc} F_c} \tag{B2}$$

where symbols used in Eq. (B2) are given below.

- $\beta_{cc} = 0.85$  (however, 1.0 when the reinforcement ratio of the compression area is 0.01 or more 1.0)
- $L_{cc}$ :it is the distance from the center to the end of the concrete compression area and is shown below.
- When  $A_{cc} \leq A_{w1}$ ,  $L_{cc} = A_{cc} / (2t_w)$
- When  $A_{cc} > A_{w1}$ ,  $L_{cc} = \frac{A_{w1}}{A_{cc}} \times \frac{L_{w1}}{2} + \left(1 - \frac{A_{w1}}{A_{cc}}\right) \left(L_{w1} + \frac{A_{cc} - A_{w1}}{2B_c}\right)$
- $t_w$ : wing wall thickness ( $mm$ )
- $L_{w1}$ : wing wall length ( $mm$ )
- $A_{w1} = L_{w1} \times t_w$ :wing wall area
- $B_c$ : column width ( $mm$ )

Shear strength of the wall element and the shear strength of the column element in Eq. (3) can be written as:



$$Q_{su} = Q_{suw} + Q_{suc} + 0.1N \tag{B3}$$

$$Q_{suw} = \left\{ \frac{0.053(p_{twe})^{0.23}(F_c + 18)}{M/(Qd_w) + 0.12} + 0.85\sqrt{p_{wh}\sigma_{why}} \right\} t_w j_w \tag{B4}$$

$$Q_{suc} = \left\{ \frac{0.053(p_{tce})^{0.23}(F_c + 18)}{M/(Qd_{ce}) + 0.12} + 0.85\sqrt{p_{cwe}\sigma_{cwy}} \right\} b_{ce}j_{ce} \quad (B5)$$

where symbols used in Eq. (B4) and (B5) are given below.

- $p_{twe}$ : tension reinforcement ratio of wall element
- $F_c$ : compressive strength of concrete ( $N/mm^2$ )
- $M/Q$ : shear span ( $0.5 \leq M/(Qd_w) \leq 2$  and  $1 \leq M/(Qd_{ce}) \leq 3$ )
- $d_w$ : effective length of column with wing walls
- $p_{wth}$ : transverse reinforcement ratio of wall element
- $\sigma_{why}$ : yield strength of wing wall reinforcement.
- $t_w$ : thickness of wing wall
- $j_w$ : distance between center of tension and compression of column with wing walls
- $p_{tce}$ : tension reinforcement ratio of column element
- $d_{ce}$ : effective length of column
- $p_{cwe}$ : transverse reinforcement ratio of column element
- $\sigma_{cwy}$ : yield strength of hoop
- $b_{ce}$ : width of column excluding the wing wall thickness
- $j_{ce}$ : distance between center of tension and compression of column element

## References

- [1] Xiao Y, Ma R. Seismic retrofit of RC circular columns using prefabricated composite jacketing. *J Struct Eng* 1997;123:1357–64.
- [2] Shin TC, Teng TL. An overview of the 1999 Chi-Chi, Taiwan, earthquake. *Bullet Seismolog Soc America* 2001;91:895–913.
- [3] DesRoches R, Comerio M, Eberhard M, Mooney W, Rix GJ. Overview of the 2010 Haiti earthquake. *Earthquake Spectra* 2011;27:S1–21.
- [4] Pessiki S, Harries KA, Kestner JT, Sause R, Ricles JM. Axial behavior of reinforced concrete columns confined with FRP jackets. *J Compos Constr* 2001;5:237–45.
- [5] Choi SW, Park SW, Park HS. Multi-objective design model for retrofit of reinforced concrete frames with infilled walls using FRP bracings. *Constr Build Mater* 2017;140:454–67.
- [6] Seo H, Kim J, Kwon M. Optimal seismic retrofitted RC column distribution for an existing school building. *Eng Struct* 2018;168:399–404.
- [7] Park K, Oh BK, Park HS, Choi SW. GA-based multi-objective optimization for retrofit design on a multi-core PC cluster. *Comput-Aided Civ Infrastruct Eng* 2015;30:965–80.
- [8] Seible F, Priestley MN, Hegemier GA, Innamorato D. Seismic retrofit of RC columns with continuous carbon fiber jackets. *J Compos Constr* 1997;1:52–62.
- [9] Reinhorn AM, Li C, Constantinou MC. Experimental & analytical investigation of seismic retrofit of structures with supplemental damping, Part 1: fluid viscous damping devices. 1995.
- [10] Cromwell J, Harries K, Shahrooz B. Environmental durability of externally bonded FRP materials intended for repair of concrete structures. *Constr Build Mater* 2011;25:2528–39.
- [11] Maheri M, Kousari R, Razazan M. Pushover tests on steel X-braced and knee-braced RC frames. *Eng Struct* 2003;25:1697–705.
- [12] Maheri M, Sahebi A. Use of steel bracing in reinforced concrete frames. *Eng Struct* 1997;19:1018–24.
- [13] Özel AE, Güneşli EM. Effects of eccentric steel bracing systems on seismic fragility curves of mid-rise R/C buildings: a case study. *Struct Saf* 2011;33:82–95.
- [14] Xiao Y, Wu H. Compressive behavior of concrete confined by carbon fiber composite jackets. *J Mater Civ Eng* 2000;12:139–46.
- [15] Dai J-G, Bai Y-L, Teng J. Behavior and modeling of concrete confined with FRP composites of large deformability. *J Compos Constr* 2011;15:963–73.
- [16] Ozcan O, Binici B, Ozcebe G. Seismic strengthening of rectangular reinforced concrete columns using fiber reinforced polymers. *Eng Struct* 2010;32:964–73.
- [17] Aboutaha RS, Engelhardt MD, Jirsa JO, Kregger ME. Rehabilitation of shear critical concrete columns by use of rectangular steel jackets. *Structural Journal*. 1999;96:68–78.
- [18] Higashi Y, M O. Anti-systemmetric loading tests on reinforced concrete columns with wing walls (Part 1). *Proceedings of AIJ annual convention 1973*. p. 1405–6.
- [19] Higashi Y, Ohkubo M. Anti-systemmetric loading tests on reinforced concrete columns with wing walls (Part 2). *Proceedings of AIJ annual convention 1974*. p. 1289–90.
- [20] Higashi Y, Ohkubo M. National research project on the prevention of brittle failure of reinforced short columns (Part 9: Tests on columns with wing walls). *AIJ Annual Convention 1974*:1305–6.
- [21] Higashi Y, Ohkubo M. National research project on the prevention of brittle failure of reinforced short columns (Part 37: Second phase tests on columns with wing walls). *AIJ Annual Convention 1976*:1417–8.
- [22] Association JBDP. Standard for seismic evaluation of existing reinforced concrete buildings. *JBDPA* 2017.
- [23] Kabeyasawa T, Kabeyasawa T, Tojo Y, Kabeyasawa T. Experimental study on columns with wing-walls failing in shear. *Proceedings of the Japan Concrete Institute*. 2008. p. 115–20.
- [24] Tojo Y, Kabeyasawa T, Kabeyasawa T, Kim Y. Experimental study on column with wing walls yielding in flexure. *Proceedings of the Japan Concrete Institute*; 2008. p. 109–14.
- [25] Seitaro T, Sawai K, Iso M. Experimental study on the shear behavior of RC columns with wing walls. *Proceedings of the Japan Concrete Institute*; 2009. p. 163–8.
- [26] Kabeyasawa T, Kim Y, Kabeyasawa T, Fukuyama H. Evaluation on flexural deformability of reinforced concrete columns with wing walls. *Performance-Based Seismic Engineering: Vision for an Earthquake Resilient Society*. 2014. p. 207.
- [27] Kabeyasawa T, Kabeyasawa T, Kim Y, Kabeyasawa T, Bae K. Tests on reinforced concrete columns with wing walls for hyper-earthquake resistant system. *Proceedings of 3rd International Conference on Advances in Experimental Structural Engineering*: Citeseer. 2009. p. 1–12.
- [28] Kabeyasawa T, Kim Y, Sato M, Hyunseong H, Hosokawa Y. Tests and analysis on flexural deformability of reinforced concrete columns with wing walls. *Proceedings of the 2011 Pacific conference on earthquake engineering (PCEE2011)*. New Zealand Society for Earthquake Engineering, Paper; 2011. p. 1–8.
- [29] Liu K-C, Liu Y-W, Huang W-C, Chen C-Y. The structure behavior of reinforced concrete wing-wall under earthquake. *Int J Phys Sci* 2010;5:1164–74.
- [30] Chang SY, Chen TW, Tran NC, Liao WI. Seismic retrofitting of RC columns with RC jackets and wing walls with different structural details. *Earthquake Eng Eng Vibrat* 2014;13:279–92.
- [31] Wen Y-K, Kang Y. Minimum building life-cycle cost design criteria. I: Methodology. *J Struct Eng* 2001;127:330–7.
- [32] Liu M, Burns SA, Wen Y. Optimal seismic design of steel frame buildings based on life cycle cost considerations. *Earthquake Eng Struct Dyn* 2003;32:1313–32.
- [33] Deb K, Pratap A, Agarwal S, Meyarivan T. A fast and elitist multiobjective genetic algorithm: NSGA-II. *IEEE Trans Evol Comput* 2002;6:182–97.
- [34] Song L. *NGPM a NSGA-II program in MATLAB*. The MathWorks: Natick, MA; 2011. p. 20.
- [35] Park HS, Lee E, Choi SW, Oh BK, Cho T, Kim Y. Genetic-algorithm-based minimum weight design of an outrigger system for high-rise buildings. *Eng Struct* 2016;117:496–505.
- [36] Dehghani S, Vosoughi A, Banan MR. The effects of rehabilitation objectives on near optimal trade-off relation between minimum weight and maximum drift of 2D steel X-braced frames considering soil-structure interaction using a cluster-based NSGA II. *Struct Multidiscip Optim* 2019;59:1703–22.
- [37] Mazzoni S, McKenna F, Scott MH, Fenves GL. *The open system for earthquake engineering simulation (OpenSEES) user command-language manual*. 2006.
- [38] Cipollina A, López-Inojosa A, Flórez-López J. A simplified damage mechanics approach to nonlinear analysis of frames. *Comput Struct* 1995;54:1113–26.
- [39] Spacone E, El-Tawil S. Nonlinear analysis of steel-concrete composite structures: State of the art. *J Struct Eng* 2004;130:159–68.
- [40] Park Y-J, Ang A-H-S, Wen YK. Seismic damage analysis of reinforced concrete buildings. *J Struct Eng* 1985;111:740–57.
- [41] Japan BCo. *Guidelines for Standard Requirements on Building Structures*. BCJ. 2007.
- [42] Liu M, Wen Y, Burns SA. Life cycle cost oriented seismic design optimization of steel moment frame structures with risk-taking preference. *Eng Struct* 2004;26:1407–21.
- [43] FEMA P. *Commentary for the seismic rehabilitation of buildings*. FEMA-356, Federal Emergency Management Agency, Washington, DC. 2000.
- [44] El-Sokkary H, Galal K. Analytical investigation of the seismic performance of RC frames rehabilitated using different rehabilitation techniques. *Eng Struct* 2009;31:1955–66.